Joint Support Command
Ministry of Defence

Impact of Methanol on the combustion process

an experimental study

Report number	FMW.MTW.2020.001
DOI:	10.13140/RG.2.2.17619.20000
Date	04 - 12 - 2020
Status	Final
Project	Green Maritime Methanol
Project number	060.37144

Colophon

	Nederlandse Defensie Academie Faculteit Militaire Wetenschappen
Location	Den Helder - KIM Het Nieuwe Diep 8 Den Helder
Mailing address	Postbus 90004 3509 AA UTRECHT MPC 55A
Contact	R.G. van de Ketterij *HL System Engineering* T 0223657415 M 0610651721 RG.vd.Ketterij@mindef.nl
Version number	01
Editor	Prof.dr.ir. R.G. van de Ketterij Ir. R. Tol Ir. J.J. Bosklopper
Based on work of	Prof.dr.ir. R.G. van de Ketterij Ir. R. Tol Ir. J.J. Bosklopper G. Doetjes BSc Dr. F.F. Vercauteren Dr. J. Eversdijk Ing. R.A.H. Reuvers Ing. C.L. Dijkstra J. Krieger Ing. M.Roberscheuten H.Sapra MSc. W. van Sluijs Dr.Ir. C.Bekdemir Dr.Ir. P. de Vos Ir. K.Visser

Disclaimer

This report is a summary of the work of Ruben Tol [Tol 2020], Jurrian bosklopper [Bosklopper 2020a; Bosklopper 2020b], Gerlof Doetjes [Doetjes 2020] and their supervising and supporting teams. The report does not reveal any new information and only summarises the information described in these works. The work is not intended to be a new work, but only serves as a summary of the work done within work package 3 of the Green Maritime Methanol project.

The different chapters in this report summarise the different reports. Parts of these reports are copied integrally in this report; in some cases edited to get some uniformity in this report.

Robert van de Ketterij

Den Helder, December 2020

1 Table of contents

1 Table of contents....4

2 Introduction....5
2.1 Background 5
2.2 Methanol use in an internal combustion engine 5

3 Dissolving methanol in diesel....6
3.1 Introduction 6
3.2 Emulsion Formation and Degradation processes 6
3.3 Emulsifiers 9
3.4 Tests 11
3.5 Conclusions 14

4 Injecting methanol in an Internal Combustion Engine....15
4.1 Introduction 15
4.2 Chemical properties of methanol 15
4.3 Methanol injection and ignition 18

5 Port fuel injection in a Spark Ignited Engine (SI-ICE)....21
5.1 The Caterpillar 3508G engine 21
5.2 Test plan 26
5.3 Test results 27
5.4 Modelling 34
5.5 Model Analyses 38
5.6 Conclusions 45

6 Direct injection of a methanol-pilot fuel mixture in a compression ignited Internal Combustion Engine (ICE)....47
6.1 The MAN 4L20/27 4 stroke compression ignited engine 47
6.2 Test plan 49
6.3 Test results 50
6.4 Modelling 57
6.5 Model Analysis 63
6.6 Conclusions 68

7 Conclusions....69

8 Future research....71

9 References....73
A.1 Description of the Measurement equipment 76

2 Introduction

2.1 Background

The maritime sector is facing a major challenge. While a globally growing economy leads to more demand for transport of goods, the goals from the Paris climate agreement and the subsequent agreement in IMO require a 50% reduction of CO2-emissions from maritime transport by 2050. Several parties are working on the development of new fuel types for shipping, such as methanol, hydrogen, various biofuels and battery-electric. There is great uncertainty about the best option for the short and longer term, and what the best options are for different ship segments [Ketterij, 2018].

Solutions for the short sea market for the short term should contribute to a significant CO2 reduction, but also should be compliant with the SECA and NECA regulations and fit within the existing layout of the ship.

The use of methanol is considered one of the most promising options for implementation in the short to medium term, based on the potential availability, emission reduction and energy density. As an energy carrier fossil-based methanol can reduce Tank-To-Wake CO2-emissions by up to 10% compared to MDO, and furthermore improve air quality emissions (SOx, NOx and PM).

2.2 Methanol use in an internal combustion engine

The chemical properties of methanol differ from the various diesel types. As a result methanol cannot be injected directly in a compression ignited internal compression engine (CI-ICE). This report focuses on possible ways to inject and ignite methanol in an Internal Combustion Engine (ICE).

We will summarise the four ways to inject and ignite methanol, and describe the experimental results of two injection methods tested within the green maritime methanol (GMM) project. For an extensive description of the experiments, experimental results and theoretical model we refer to [Bosklopper, 2020a; Bosklopper 2020b; Tol 2020]. The report does not contain any new information compared to these three references. Large parts of the reports and paper have been taken over in this summarizing report integrally.

One of the methods described involves direct injection of a methanol-diesel mixture in the cylinder. Methanol and diesel do not mix and do not dissolve. Direct injection of a mixture therefor requires an active methods to keep both chemical compounds mixed at a pre-defined rate. We tested use of emulsifier, described in [Doetjes 2020] and active mixing in a day tank.

3 Dissolving methanol in diesel

3.1 Introduction

Methanol does not ignite easy in a compression ignited engine. To overcome this problem a pilot fuel is required that starts the combustion process after which the methanol air mixture ignites. The pilot fuel can be mixed with methanol or injected separately in the cylinder.

As it is our objective to research the combustion process of methanol with a minimum of adaptations to the engine, one of the lines of research is to inject a mixture of methanol and pilot fuel in the cylinder.

In order to keep this process stable the pilot fuel concentration in methanol (or methanol concentration in the pilot fuel) cannot vary much. This imposes strict requirements to the mixture, and preferably we aim for dissolving one fuel in the other.

Our prime pilot fuel is however F76, a fuel with characteristics that prohibit methanol to dissolve in F76. Both fuels will separate in time as result of four degradation processes: Ostwald ripening, aggregation processes, phase separation, and phase inversion. We attempted to slow down these processes to obtain a solution that remains stable for 8 hours or longer.

We tested a number of emulsifiers to observe stabilization time. To keep the impact of the emulsifier on emissions to a minimum, we used in all cases 0,3 weight volume % of emulsifier.

3.2 Emulsion Formation and Degradation processes

An emulsion consists of two fluids that will not naturally mix or dissolve. In case of methanol and diesel the two fluids will not dissolve as polarity of the fluids are not equal. Polarity of a fluid is the result of a separation on molecular scale of electric charge. This leads to the molecules having a negatively charged end and a positively charged end. Methanol is a polar molecule which in this situation results from the OH-group. When mixing methanol with another polar fluid, the positive and negative ends of the different molecules will attract, enabling the two fluids to dissolve.

Unfortunately diesel consists of Carbon atoms connected to hydrogen atoms or other carbon atoms. Both ends of the resulting molecule are equal and consequentially the molecule is apolar. The molecules do not have a dipole moment, and will not attract to the polar methanol molecules.

An emulsion can be formed in three ways: the two phases can be mixed by high shear mixing or by ultrasonic emulsification. Finally we can try to overcome the surface tension.

In the degradation process of emulsions four processes play a role: phase separation, Ostwald ripening, aggregation processes and phase inversion (Figure 1).

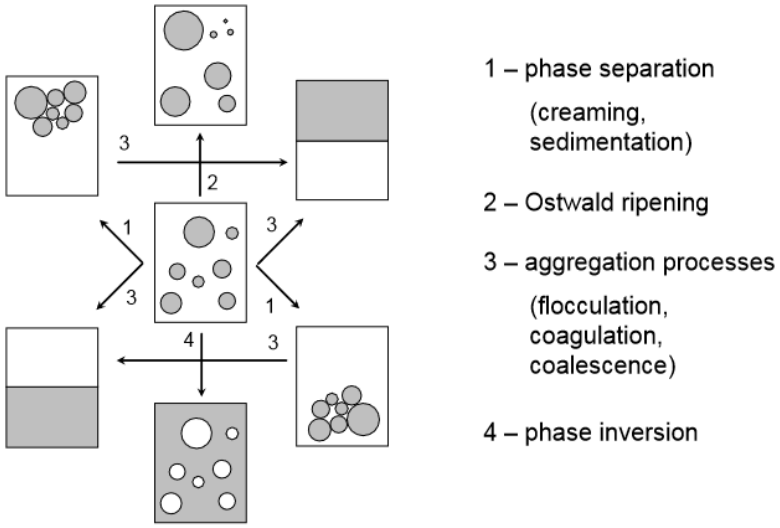

Figure 1: Degradation processes of emulsions

3.2.1 *Phase separation*

Under influence of gravity and differences in specific density, the phases in an emulsion will separate leading to two different layers. The disperse phase may either settle under (sedimentation) or float on top of (creaming) the continuous phase depending on the specific gravity of the disperse phase with respect to the continuous phase.

The specific density of methanol is lower than that of F76 so in this case methanol will cream. The speed with which creaming occurs, depends on the size of the methanol droplets in F76. The smaller the droplets are and the longer they remain small, the longer it will take for methanol to cream on top of F76.

Creaming can also be delayed by continuous device of the two phases where the higher layers in a tank are forced back to the tank bottom by a stirring device.

3.2.2 *Droplet growth*

As stated in previous paragraph. It is important to keep droplet size as small as possible for a maximum period. To minimize droplet growth we first have to understand the way droplets grow and then try to intervene in this process. We will briefly describe the different ways droplets grow.

Ostwald Ripening

If the surface tension of a droplet in an emulsion equals γ, the overpressure within the droplet equals: $dP \approx \frac{2\gamma}{r}$.

Where:

dP	= overpressure in a droplet	[N m-2]
γ	= surface tension of a droplet	[N m-1]
r	= droplet radius	[m]

The overpressure will therefore be increase with decreasing droplet size. The molecules on the surface are less stable than the molecules in the interior as they have less neighbors they can attract to. As result of the higher overpressure inside smaller droplets, the molecules on the surface of small droplets will be less stable than the molecules on the surface of large droplets, and there are relatively more molecules at the surface of small droplets than on the surface of large droplets.

All molecules at the surface of all droplets tend to detach from the droplets and diffuse in the solution. However this process proceeds in a faster rate for smaller droplets. These individual droplets, when the free molecules in the solution become supersaturated, tend to condense again on the surface of droplets, where larger droplets are favored over smaller droplets.

As a result, smaller droplets tend to shrink in time, where larger droplets grow. This process is shown in Figure 2.

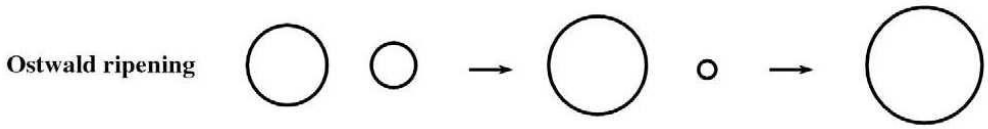

Figure 2: Ostwald ripening within an emulsion

Aggregation processes (flocculation and coalescence)

When flocculation (Figure 3) occurs the droplets of the disperse phase will aggregate without corroding the surface of the droplets. Flocculation speeds up the creaming process because flakes of droplets rise (or sink) more rapidly than individual droplets.

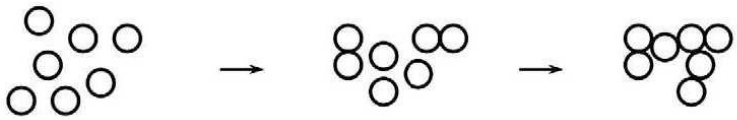

Figure 3: Flocculation process in an emulsion

Flocculation speed depends on the size of the van der Waals forces, electrostatic and steric forces. The Van der Waals forces depend for a given molecule on droplet radius and the surface-to-surface distance between the droplets. The van der Waals forces are counteracted by electrostatic forces and steric forces.

According to Doetjes the steric forces in the methanol-diesel are mixtures the most important forces counteracting the van der Waals forces, although electrostatic stabilization of the droplets is also possible.

Once the droplets cluster the boundaries between the droplets disappear and form a single daughter droplet of larger dimensions (Figure 4). This process is referred to as coalescence. In order for coalescence take place, the droplets must contact each other.

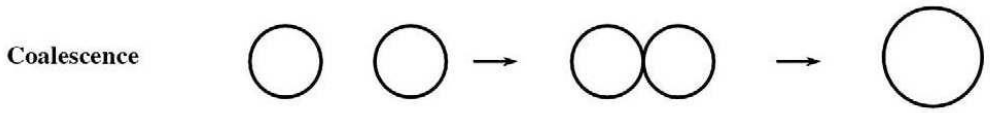

Figure 4: Schematic representation of the coalescence process.

3.3 Emulsifiers

Emulsifiers can intervene in different phases of the emulsion formation process and degredation process, enhancing mixture stability and delaying degradation processes. We will briefly describe the operation principles of emulsifiers and more particularly the emulsifier chosen by Doetjes [Doetjes 2020].

Apolar fluids tend to separate from water and are called hydrophobic or lipophilic fluids. Polar fluids dissolve easily in water and are called hydrophilic fluids. Emulsifier consists of long molecules with a hydrophilic head and a hydrophobic tail (Figure 5). The idea behind use of an emulsifier during mixture formation is that the head connects to the methanol molecule (both being hydrophilic), where the tail connects to diesel (both being hydrophobic). In this way a more stable mixture is formed and surface tension can be reduced.

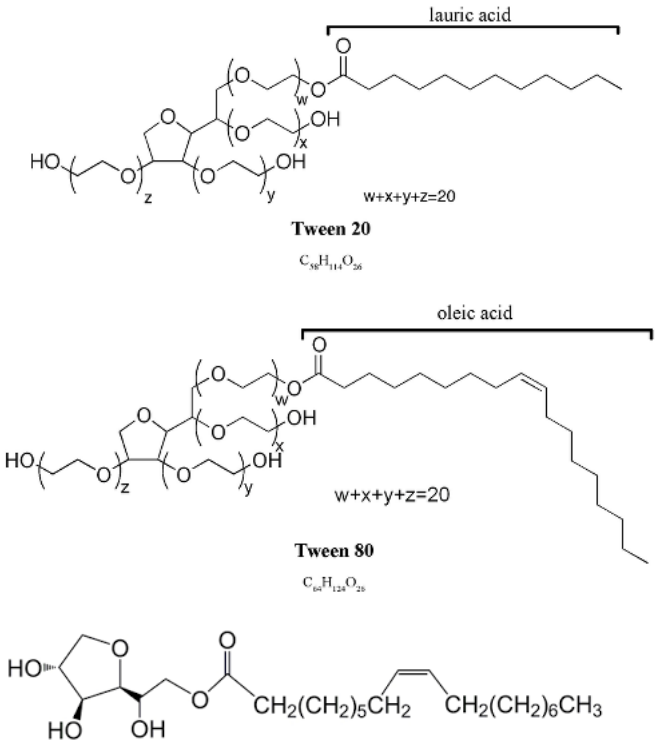

Figure 5: Top Tween 20: HLB16; Middle: Tween 80: HLB15 and Low: Span80: HLB4

The HLB value represents the ratio between hyrdrophilic and hydrophobic components of the emulsifier. An emulsifier with a low HLB value has a lypophilic (hydrophobic) characteristic. A high HLB value means the emulsifier has a hydrophilic characteristic.

The rate of success of an emulsifier, given the concentration and character of the disperse phase, is governed by the HLB (Hydrophylic – Lypofilic Balance) and the concentration of the emulsifier. The emulsifier tested by Doetjes consisted of Tween and Span surfactants. The rate of success of an emulsifier is governed by the HLB (Hydrophilic – Lyophilic Balance) and the concentration of the emulsifier.

Based on literature [Jiao 2016], Doetjes concluded a HLB value of 5,4 would result in maximum stability of 90 % (volumetric) F76 and 10 % (volumetric) methanol. A higher methanol content would in any case decrease stability of the mixture.

Emulsifiers intervene the process of droplet growth and phase separation in different phases. Impurities with poor solvability characteristics with respect to the continuous phase and strong attraction to surface of the disperse phase decelerate the Ostwald ripening process. The impurities will position on the surface of the disperse phase and will be absorbed by the surface of the disperse phase. As result the individual molecules will have more difficulties contacting the larger droplets. Also it becomes impossible for different droplets to directly connect each other.

Without any force counteracting the van der Waals forces the entire disperse phase will aggregate to a single zone. An emulsifier can create a steric or electrostatic force counteracting the van der Waals force. Electrostatic forces arise from polarity differences where steric forces arise from overlapping of long molecules in a small volume. The long molecules become fixated in the decreasing volume between two droplets as they approach. Figure 6 [Tadros, 2016] shows schematically how steric stabilization works. Figure 7 [Ayouril 2011] schematically shows the working principle of electrostatic stabilization.

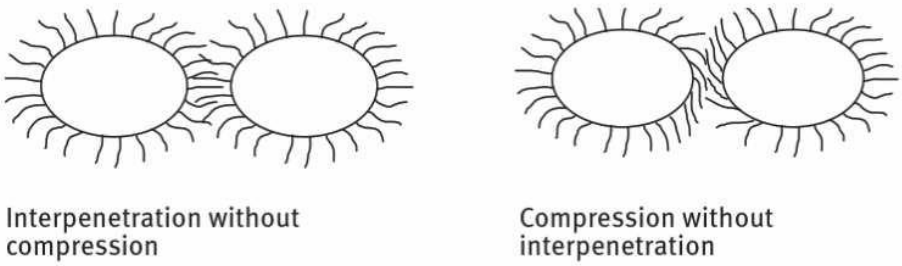

Figure 6: two possible steric stabilization possibilities

Steric forces are the most important forces counteracting the van der Waals forces. When two droplets approach, the long molecules from both droplets will more and more interact resulting in increasing repulsive forces with reducing distance between two droplets.

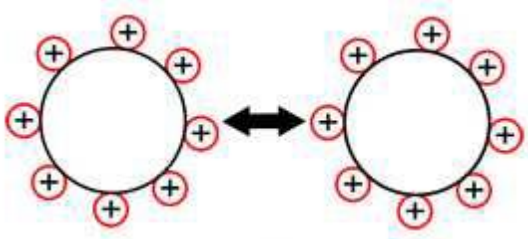

Figure 7: electrostatic stabilization

3.4 Tests

Advised by TNO [Eversdijk 2020] we tested the following emulsifiers:

1. BYK-W 9010
2. TWEEN 80
3. SPAN 65
4. PLURONIC P-123
5. PLURONIC L-121
6. HYPERMER B246-SO-(MV)

The mixture we considered had a ratio of 90% F76 and 10 % methanol (weight). The volume tested was 50 ml. We used a emulsifier volume of 3 % of the methanol volume. The tests therefore consisted of a mixture of:

- 89.73 wt% F76
- 9.97 wt% methanol
- 0.299 wt% emulsifier

3.4.1 Small scale tests results

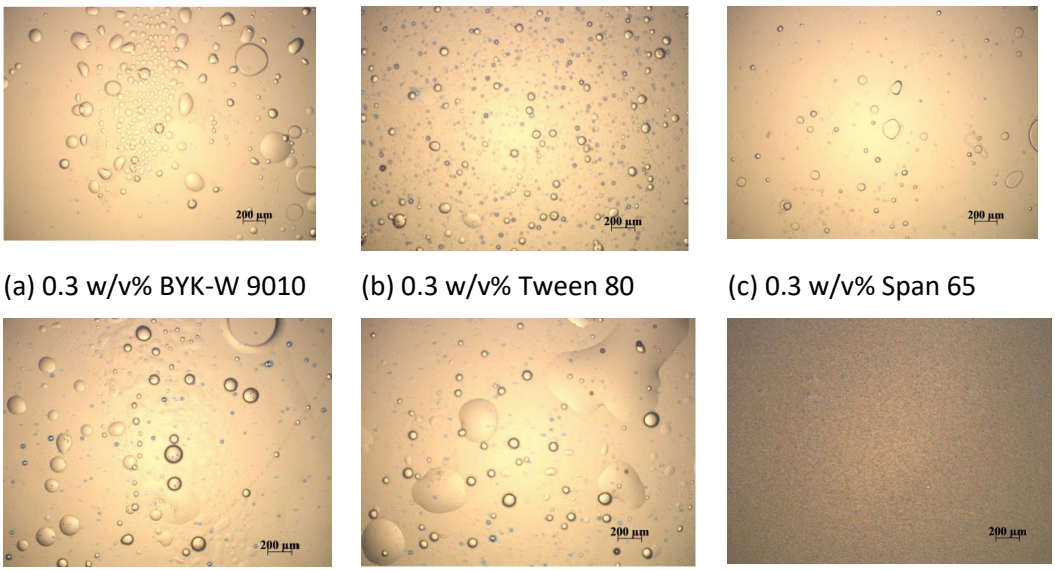

(a) 0.3 w/v% BYK-W 9010 (b) 0.3 w/v% Tween 80 (c) 0.3 w/v% Span 65

(d) 0.3 w/v% Pluronic P-123 (e) 0.3 w/v% Pluronic L-121 (f) 0.3 w/v% Hypermer B246-SO-(MV)

Figure 8: droplet size small scale tests after stirring for 5 minutes at a speed of 4000 rpm

We mixed the fluids using an overhead stirrer, mixing the fluids at a speed of 4000 rpm during 5 minutes, and with an ultrasonic homogenisator which added 4800 J of energy to the mixture in 2 minutes.

Figure 8 shows the results of the small scale tests after stirring for 5 minutes at a speed of 4000 rpm. Hypermer B246-SO-(MV) has the smallest droplet size and seems the best candidate. Also tween80 has a good result, with droplet size sufficiently small to enable stable injection and combustion. Hypermer B246-SO-(MV) remained stable for around 10 hours.

The tests with ultrasonic homogenization revealed equivalent results, but droplet size was smaller cases (a), (b), and (c).

3.4.2 Tests at larger scale: 5 liters

After small scale testing we continued on a larger scale of 5 l. The tests performed were done with a mixture of TWEEN and SPAN (see Table 1). We could not obtain sufficient amounts of Hypermer B246-SO-(MV) on time for doing larger scale tests.

We used a mixture of ratio of 74.4% Span 65 and 25.6 % Tween 80. This resulted in an emulsifier with a HLB value of 5,4 which we, after consultation with TNO, considered optimum for a mixture with 10 % methanol.

Table 1: Characteristics of SPAN65 and TWEEN80

Properties	Span 65	Tween 80
Chemical composition	$C_{60}H_{114}O_8$	$C_{64}H_{124}O_{26}$
Producer	Sigma-Aldrich	Sigma-Aldrich
Appearance	Light cream	Yellow
Physical form	Powder	Liquid
pH	-	5-7
Density (25°C; g/cm^3)	0,98	1,07
HLB	2,1	15
Flash point (°C)	149	149

In order to get sufficient energy in the mixture we used a high speed overhead mixer [ULTRA-TURRAX T18 digital] at a speed of 17400 rpm (Figure 9). We reduced the emulsifier with a factor 10 to 0,3 % of the methanol weight.

Figure 9: 5 liter test set-up

We did vary the composition of Tween and Span for confirmation of our assumption on the optimum ratio, and mixing time and took samples after leaving the solution calm for 5, 10, 15, 30 and 60 minutes. We took close-ups of the mixture under a microscope. We also tested the flash point of the mixture at these moments, to see in how far we still had a mixture composed of diesel and methanol.

The test naming is described by: $M_{10}E_{0.3}S_{74.4}T_{25.6}ST_5TRT_5$. In this naming:

- M_{10} refers to the methanol percentage
- $E_{0.3}$ refers to the emulsifier percentage
- $S_{74.4}$ refers to the percentage Span 65 (in the Span-Tween mixture)
- $T_{25.6}$ refers to the percentage Tween80 (in the Span-Tween mixture)
- ST_5 is the resting time of the mixture in minutes
- TRT_5 is the mixing time of the mixture in minutes

The ratio of 74.4% Span 65 and 25.6 % Tween 80 gave an emulsifier with a HLB value of 5,4 which is optimum for a mixture with 10 % methanol.

3.4.3 *Results*

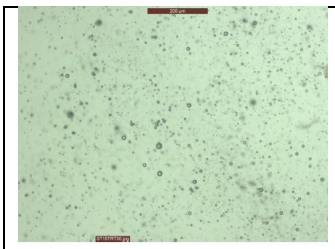	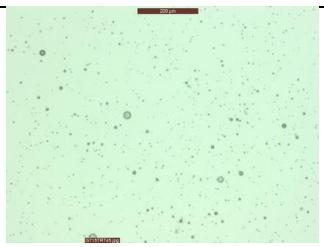	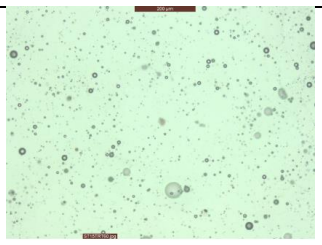
(a)ST15TRT30	(b)ST15TRT45	(c) ST15TRT60

Figure 10: droplet size of $M_{10}E_{0.3}S_{74.4}T_{25.6}$ after (a) 30 minutes; (b) 45 minutes; (c) 60 minutes stirring. Resting time was 15 minutes. The red beam on top has a length of 200 μm.

Figure 10 shows the development of the droplet size after stirring for increasing duration using a magnetic stirring device. Comparison with Figure 8 shows comparable droplet size. Apparently we need more stirring time (it seems 30 minutes stirring time is sufficient and optimum) to obtain comparable droplet size of methanol in F76.

We observed carefully the separation process after stopping the mixing process. Irrespective of the mixing time separation took only about 10 minutes. After 10 minutes methanol was completely separated from F76.

As the magnetic stirring procedure did not produce satisfactory results we started using the set-up of Figure 9. The droplet size became significantly smaller. Again the mixture was not stable and separation process was completed within half an hour.

An increase of the emulsifier content with a factor 10, up to 3 % weight % of the total volume did result in a more stable solution: after stirring for 45 minutes and a resting time of 15 minutes, methanol droplet size was of the order of magnitude of 10 – 20 μm. When stirring for 60 minutes the solution was stable with a methanol droplet size of around 10 μm. However, at a stirring time of 60 minutes a significant amount of methanol had evaporated from the mixture.

Although the solution remained stable for longer duration, separation process was finished after about 4 hours in any case.

3.5 Conclusions

- The results of the tests show that a stable emulsion appears when Hypermer B246-SO-(MV) (0.3 w/v%) is used. This emulsion remained stable for more than 10 hours
- This emulsifier is also the only one that could accomplish this result. Because of the small amount of emulsifier Hypermer B246-SO-(MV) pointed out to be quite effective.
- Our tests with Span 65 and Tween 80 (0,3 w/v%), in ratio 74,4:25,6 w% indicate that a small droplet size can be obtained, but the resulting mixture did not remain stable for longer periods
- Literature studies [Jiao 2016] and tests with Span 65 and Tween 80 (3 w/v%), in ratio 74,4:25,6 w% indicate that a small methanol droplet size can be obtained, and the resulting mixture remained stable for up to 4 hours.
- During the mixing process part of the methanol evaporates. For mixing durations over 45 minutes, this evaporation process removes a major part of the methanol.

4 Injecting methanol in an Internal Combustion Engine

4.1 Introduction

There are four different ways to inject and combust methanol or a methanol diesel mixture in an internal combustion engine. We will briefly describe these methods. Two out of four methods were tested within the Green maritime Methanol project.

4.2 Chemical properties of methanol

Methanol is an alcohol and alcohols have deviating properties compared to convetional hydrocarbon fuels such as marine diesel oil. Table 2.1 provides the chemical properties of marine diesel oil (F-76) and methanol.

The *lower heating value* of a fuel is the amount of energy released during combustion of one kilogram of that specific fuel without taking the condensation heat into account. Methanol contains less than 50% of the energy of the same energy of the same amount of F76. As a result, the specific fuel consumption (SFC) increases when using methanol/diesel blends at a constant engine load.

The fuel *hydrogen content* has a positive impact on the combustion. High hydrogen content contributes to the flammability and ignition characteristics [Ali, 1993]. As methanol has 0.6 [weight %] lower hydrogen content, we expect slightly reduced ignition properties since as compared to F76.

The *carbon content* relates directly to the CO2 and CO emissions. It also plays an important role in the formation of particulate matter [PM] and number of particles [NP] emitted after combustion. Less carbon content is therefore advantageous for the reduction of harmful emissions if an alternative fuel contains less carbon.

The *carbon content* of methanol is almost 57% lower than that of F76. In view of the reduced Lower Heating Value we expect a net reduction of CO2 emission from the combustion process, provided the efficiency remains equal. The carbon/hydrogen (C/H) ratio of methanol is over 50% lower.

Sulfur contributes to the emissions of sulfur oxides (SO_x). The amount of sulfur in F-76 is already low due to the strict regulations for ship exhaust gas emissions. A potential disadvantage of reduced sulfur content is the elimination of the lubrication effect. On existing engines, the fuel pump is often lubricated by fuel. Diesel and methanol both have none or very low sulfur content. Lubrication effects already are very low and we therefore do not expected that low sulfur content related problems will suddenly occur by using alcohol diesel blends. Moreover, the exhaust gas emission of sulfur oxides will automatically decrease by adding less sulfur to the engine.

Oxygen from the air mixes with fuel in the cylinder and is used in the combustion process. When using diesel all oxygen needed for combustion in a diesel engine comes from the air inlet. Methanol contains an oxygen molecule in its hydroxyl

group, which helps in reaching a more complete combustion during the expansion stroke.

The fuel *density* is the mass to volume ratio of a fuel. Fuel density in combination with LHV is important in a practical way. Multiplying these two gives the amount of energy storage in the fuel tanks and relates directly to the vessels' range. Methanol has a 6.8 [%] lower density compared to diesel. As mentioned before, the LHV is also lower than that of F76. We need a higher fuel flow to produce an equal amount of power from an engine. This means that for practical applications existing fuel injectors needs to be replaced to inject a sufficient amount of fuel into the cylinders.
Assuming an identical engine running on pure methanol or methanol/diesel blends, the range of a vehicle will decrease without adapting the fuel storage capacity, resulting in an operational disadvantage when using methanol as primary fuel. Less energy storage means reduction of fuel supply independency, which results in more frequent visits to harbors or tankers

Table 2: Fuel properties F76 and Methanol (taken from Tol, 2020)

Parameter	Unit	F-76	Methanol
Lower heating value	[kJkg^{-1}]	42580	20270
Hydrogen content	[wt.%]	13.1	12.5
Carbon content	[wt.%]	86.6	37.5
Sulfur content	[wt.%]	0.05	0
Oxygen content	[wt.%]	0	50
Density	[kgm^{-1}]	847.4	790
Kinematic Viscosity 313.15 [K]	[cSt]	3.00	0.58
Flash point	[K]	342.65	284.15
Boiling temperature	[K]	463.15-553.15	337.85
Autoignition temperature	[K]	527.15	737.15
Cetane number	[-]	45.1	4
Stoichiometric AFR	[-]	14.47	6.66
Heat of Vaporization	[MJkg^{-1}]	0.27	1.11

Viscosity is an important parameter for fuels in a compression ignited (CI) engine since higher viscosity relates to better ignition properties [Stapersma, 2003]. A lower viscosity influences the spray angle in the cylinder, where spray angle reduces with viscosity. A low viscosity could cause damage to sub systems of the engine, for instance to fuel pumps and injectors. Methanol's viscosity is lower than conventional diesel fuel.

The *heat of vaporization* of a fuel indicates how much energy is needed to evaporate a kilogram of that fuel. The required heat comes from the surrounding air in the cylinder of an engine. The evaporation process results in a decrease of the temperature of the air surrounding the methanol droplets in the cylinder. This effect

is positive the formation of NOx as NOx formation increases rapidly when cylinder temperatures exceed a critical value. A variation of the temperature relates directly to the thermal efficiency of the combustion process in the cylinder.

The *heat of vaporization* of methanol is almost 4 times higher compared to diesel. As a result the in-cylinder temperature at the start of the in-cylinder process decreases before start of combustion when liquid methanol is injected. According to literature, this early stage cooling effect improves the brake thermal efficiency of the in-cylinder process [Sagarwal, 2019; Huang, 2004].

A potential disadvantage is that not all methanol will be evaporated on time. This can have significant negative consequences on the ignition process. Potentially, not all methanol will evaporate and ignite on time, leading to excessive release of unburned hydrocarbons [UHC]. Also late ignition will increase and potentially, the mixture may become too lean to ignite, leading to misfire at low engine loads.

The *flash point* of a fuel is the temperature at which the fuel vapor above the liquid bulk ignites with a lighter. This is an important parameter for the safety on board of a ship [Stapersma, 2003]. Methanol has a low flash point which could be a problem on ships.

Storage and transport on board will have an important impact on the ship design. This impact is subject of work package 5 of the *Green Maritime Methanol* Project.

The *boiling point* of a fuel is the temperature at which the fuel starts to boil. The boiling temperature of methanol, is low compared to diesel. A low boiling point needs to be considered when a fuel storage room could reach high temperatures. Therefore it has an impact on the ships' ventilation systems to regulate the temperature in this areas and to prevent flammable gases to reach the lower explosive level.

The auto-ignition temperature is important within a diesel engine. Methanol has a very high auto-ignition temperature. This will have a serious impact on the combustion process and is one of the major reasons to investigate external means to ignite the air-fuel mixture in the cylinder.

The *cetane number* identifies the fuels flammability. Low cetane number fuels have difficulties with auto-ignition and smooth combustion. In compression ignited engines, fuel is ignited by auto-ignition at a certain pressure. Low cetane fuels have higher auto-ignition pressures and temperatures, which are difficult to reach with the current compression ignited engines due to limitations of the engine's material and cylinder stiffness and strength. Methanol has a low cetane number, indicating problematic ignition in a CI engine. Therefore, methanol must be ignited by other means, such as a pilot fuel with a high cetane number, or a spark.

Due to the higher heat of vaporization and cetane number, methanol/diesel blends are expected to show a larger ignition delay compared to diesel fuel.

4.3 Methanol injection and ignition

Due to the low cetane number and high auto ignition temperature 100% methanol (M100) cannot be ignited in standard compression ignition engines. The gas fuel mixture has to be somehow ignited. Ignition can be activated using a spark, or using a pilot fuel.

As methanol has a high heat of vaporization, the in-cylinder combustion process may be negatively influenced. To overcome this problem methanol could be injected via the air injection port. This gives time for the methanol droplets to evaporate in the air. Additional advantage is that part of the heat added to the air when pressurizing the air in the turbo, can be beneficially used. The injected air can cool down to 15°C (the condensing temperature of methanol in air), reducing the starting temperature of the in-cylinder process. This has a positive impact on the efficiency of the in-cylinder process and decreases NOx formation.

Methanol could be directly injected into the cylinder. In this case pilot fuel could be directly injected with the methanol or separately. The latter injection method offers some additional potential to optimize the combustion process in the cylinder.

Summarizing, we have four main options to inject and ignite methanol in an internal combustion engine.

Figure 11 gives a schematic overview of the port-fuel injection and spark ignition process. After the exhaust stroke stroke when the exhaust valve has closed, the inlet valve opens and the (partly evaporated) methanol – air mixture enters the cylinder. Near the end of the inlet stroke, the inlet vale closes and during the compression stroke pressure and temperature build up. The remainder of the fluid methanol evaporates. Around 20° BTDC a spark is given (the optimum moment is one of the research questions) and the air-methanol mixture ignites resulting in a steep increase of the pressure. After this the work stroke follows.

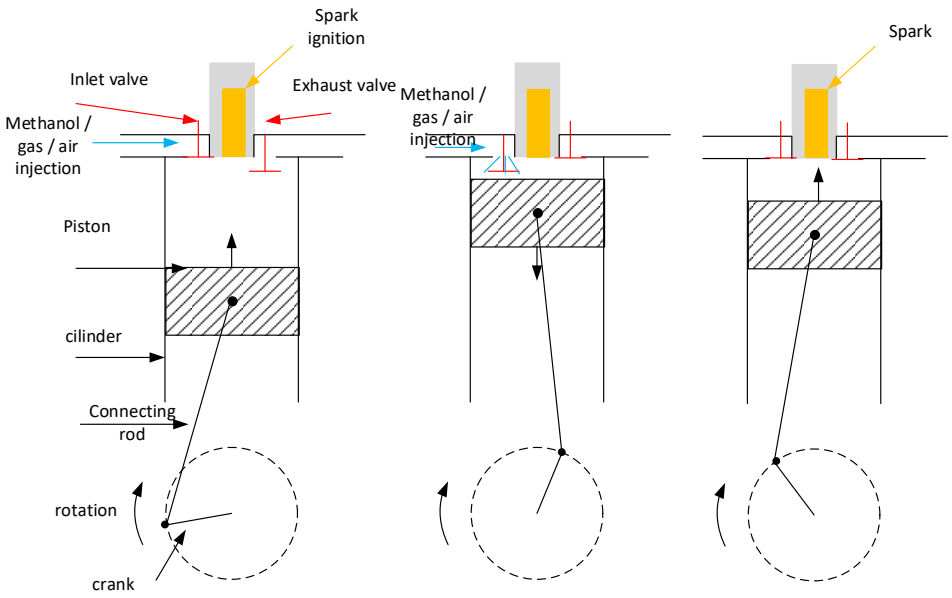

Figure 11: Schematic overview of the port-fuel injection and spark ignition process

Figure 12 shows the second option we have. The direct methanol-pilot fuel injection method, if it works, requires the least adaptations to a normal compression ignition engine.

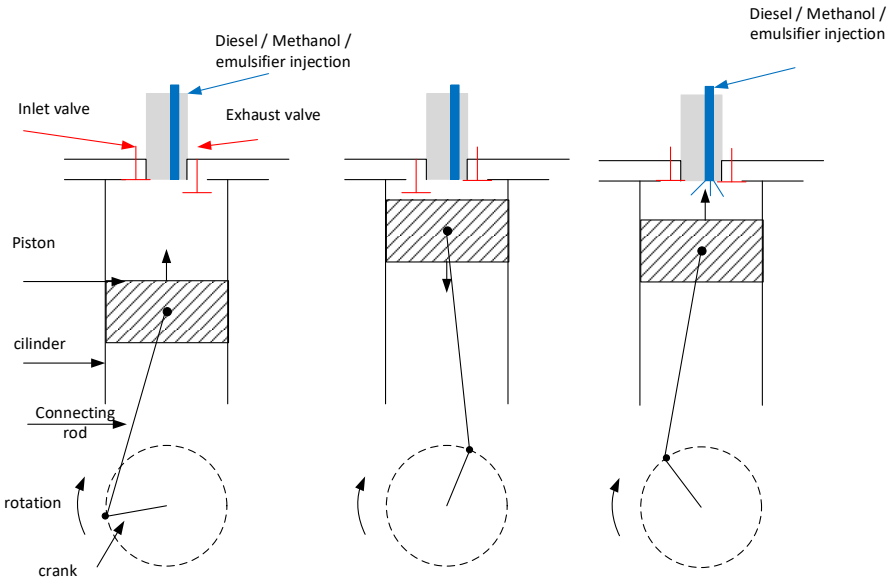

Figure 12: Schematic overview of the direct injection of a methanol-pilot fuel mixture

A mixture of methanol and pilot fuel (in this case diesel) is injected directly in the cylinder. The injection process is that of a classical compression ignition engine. Ignition is started by the auto-ignition of the pilot fuel and after the pilot fuel ignites, the methanol / air mixture follows.

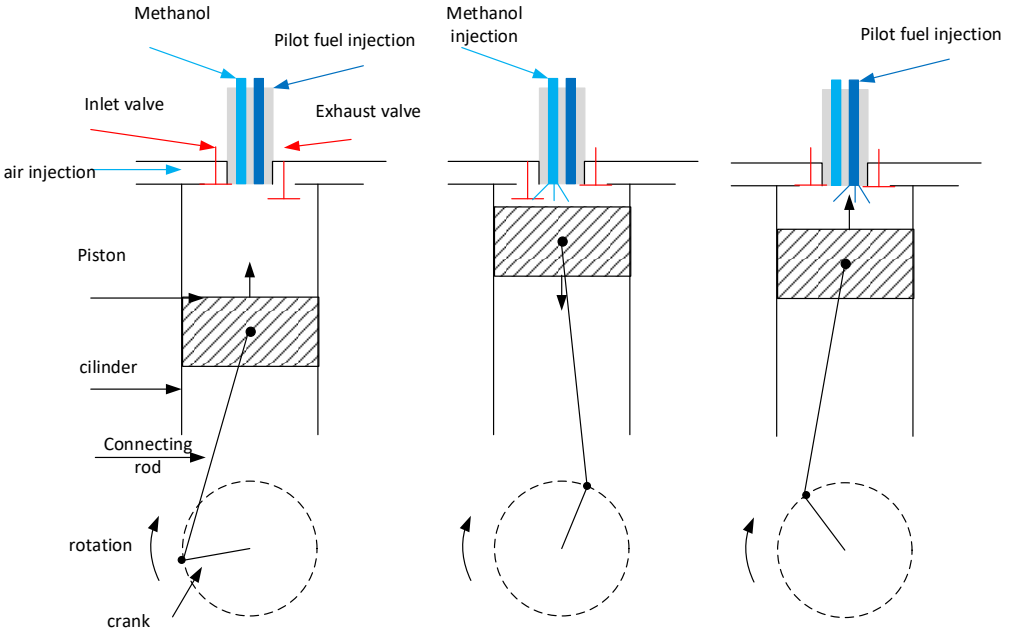

Figure 13: Schematic overview of the direct injection of methanol and separate pilot fuel

Figure 13 shows a more advanced injection concept. The direct separated methanol-pilot fuel injection allows separate injection of methanol and a pilot fuel.

During the first phases of the compression stroke methanol is directly injected in the cylinder. This gives the methanol some time to evaporate and mix well with the air in the cylinder. Near the end of the compression stroke an explosive air/methanol mixture has formed in the cylinder that only needs an excuse to ignite. At that moment a small amount of pilot fuel is injected and ignites, enabling combustion of the methanol/air mixture.

This method requires a significant reconstruction of existing engines or even a complete redesign. Smaller engines may not have sufficient space in the cylinder head for the two required injection needles for pilot fuel and methanol.

Finally Figure 14 reveals schematically the methanol port fuel injection direct injected pilot fuel method. The method is a copy of the method shown in Figure 14 but now ignition is started by a pilot fuel directly injected in the cylinder.

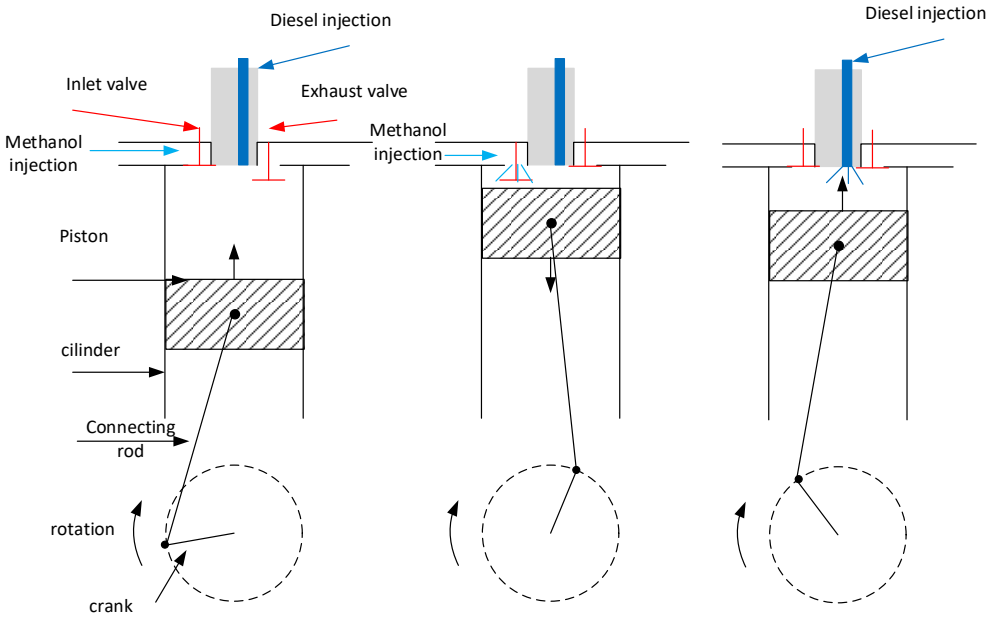

Figure 14: Schematic overview of the port fuel injection of methanol in a pilot fuel ignited ICE

Within the Green Maritime Methanol project we have tested the methods shown in Figure 11 and Figure 12.

5 Port fuel injection in a Spark Ignited Engine (SI-ICE)

For this study we used a spark ignited engine, where methanol is injected with the air via the air inlet valve, and ignited with a spark. Figure 11 shows how the process works in this engine. Similar research has been performed by Ghent university on a converted VW TDI Diesel engine with a 19,5:1 compression ratio[25].

5.1 The Caterpillar 3508G engine

Figure 15 shows the Cat 3508G-SI engine during the tests at PON in Papendrecht. The main parameters are described in Table 3.

Figure 15: The Caterpillar 3508G-SI engine at the test set-up in Papendrecht

Table 3: Main parameters of the CAT 3508G-SI engine

Parameter	Value	Units
Number of cylinders	8	-
Bore	170	mm
Stroke	190	mm
Displacement	34.5	L
Rated speed	1500	rpm
Rated Power	500	kW
Compression ratio	12:1	-
Boost pressure	2.2	bar
Cycles	4	-
Firing order	1-2-7-3-4-5-6-8	-
Inlet valve open (IVO)	8.7	^{0}CA ATDC
Inlet valve close (IVC)	21.5	^{0}CA ABDC
Exhaust valve open (EVO)	20.1	^{0}CA BBDC
Exhaust valve close (EVC)	11.8	^{0}CA BTDC
Geometry of piston bowl	Centric hemispherical combustion chamber (HCC)	-
Volume of piston bowl	250	cm^3

5.1.1 *Engine modifications for safe operation with methanol*

(This paragraph is copied from [Bosklopper 2020b].) Several systems on and around the engine were modified for safe operation and measurements with 100% methanol. The following systems are retrofitted on the CAT G3508A SI engine to operate a 100% methanol engine with port fuel injection (PFI):

System changes:

- Modified fuel system
  The modified fuel system includes modifications to fuel storage, fuel pump, filters, piping, special designed fuel rail, adjusted PFI system with high flow methanol injectors and valves. Methanol is corrosive to aluminum alloys, therefor chemical resistant materials such as stainless steel and rubber are used. The stainless steel fuel rail and the port fuel injection system are shown in Figure 16.
- Modified charged air cooling system
  New three-way valve and a modified charger air cooling control system were installed to control the temperature after the cooler. The standard system on the engine allows for constant temperature regulation after the cooler. However, the air temperature after the air cooler could not be kept constant with methanol injection. Due to the high evaporation energy requirements of methanol, the temperature after fuel injection at inlet port is load dependent. The modified charge air cooling system was installed because of concerns of reaching operating limits with the previous constant temperature regulator after the cooler at higher loads.
- New designed control system to control the fuel flow, air flow, engine speed, etc.

(a) (b) (c)

Figure 16: The modified fuel system of methanol including a double walled stainless steel fuel rail (a), injector housing for PFI (b) and the used 2200 cc/min injectors (c).

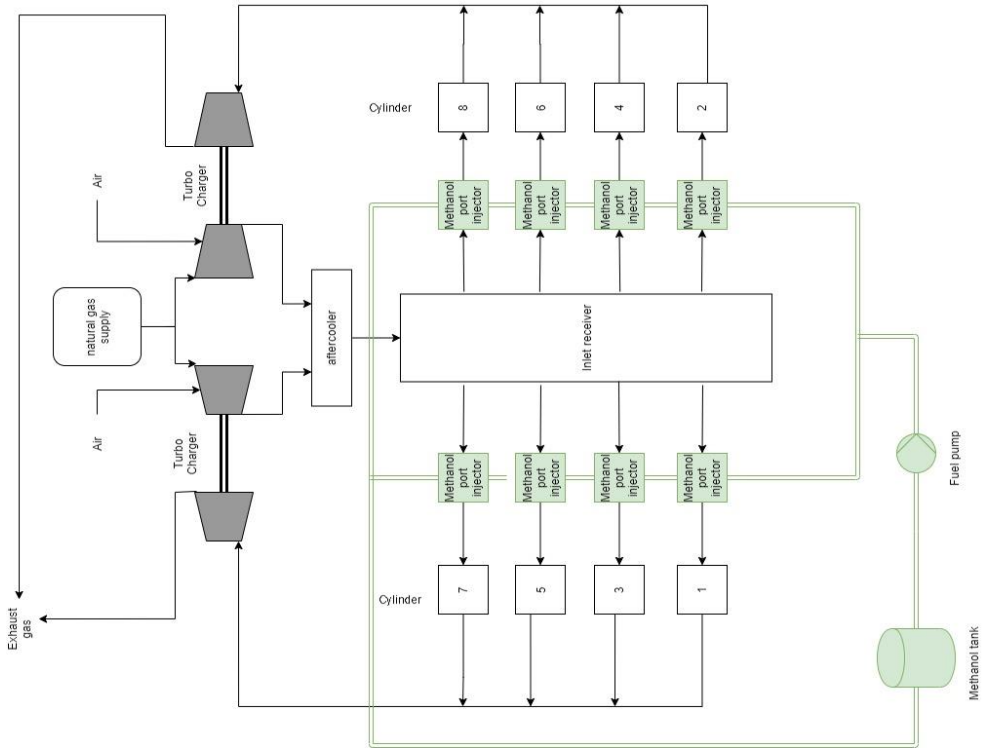

Figure 17: Schematic overview of the test set-up.

Safety measures:

- We installed two continuous methanol vapor detectors capable of measuring methanol content from 0-1000 ppm. Such a detection system was necessary because methanol is toxic to humans beyond 200 ppm. Furthermore, human senses can detect methanol only when the concentration exceeds 10 times the 200 ppm safe limit [Methanol Institute 2008].
- A fire detection system capable of detecting alcohol fires inside the test bed and outside at the fuel tank was installed.
- A nitrogen inert gas system was installed to reduce the amount of oxygen present in the fuel system and to clean the fuel system.
- Emergency stop buttons and the vapor detection systems were connected to the control system to instantly stop the engine and the fuel pump.

Measurements Equipment:

- A Testo-350 is used for exhaust gas measurements
- A Kibox 2893A is used for crank angle and in-cylinder pressure measurements.
- A Dewetron Dewe-2600 is used to collect and store all sensor data excluding the Kibox data.

The testo-350 and Kibox 2893A are used for both the experiments with the spark ignited engine and with the MAN compression ignited engine. They are described in the appendix. Figure 4 shows the engine test setup schematic with natural gas (NG) injection (for 100% NG operation), and methanol injection through port injectors (shown in green). The fuel filters, pressure sensors and valves are left out of the overview for simplicity. Both fuel supply systems can operate simultaneously.

5.1.2 Charged air cooling system

The charged air cooling system on the G3508A SI NG engine includes an aftercooler, which is placed after the compressors and before inlet receiver. The aftercooler cools the hot compressed air (and natural gas when operating on natural gas). The original regulator will designed to keep the combined air and natural gas flow in the receiver at a temperature of 35°C. The air cooling system is separate from the internal engine cooling system.

But for running the engine on methanol modifications are made on the charged air cooling system. Due to the PFI the temperature of the air inlet will be changed just before the cylinder inlet valve. This temperature change is significant due to the high heat of vaporization of methanol. The air temperature could not be kept at a constant value after the air cooler because with methanol injection the temperature after the air cooler is load dependent. Therefore, a three-way valve was installed before the cooler instead of the previous constant temperature regulator. The three-way valve was opened and closed by an electric motor, which was regulated by a PLC. With the three-way valve the cooling water flow to the air cooler was controlled, thus controlling the manifold temperature. The three-way cooling valve, the electric motor and the control system cabinet are shown in Figure 18 (a) and (b) respectively.

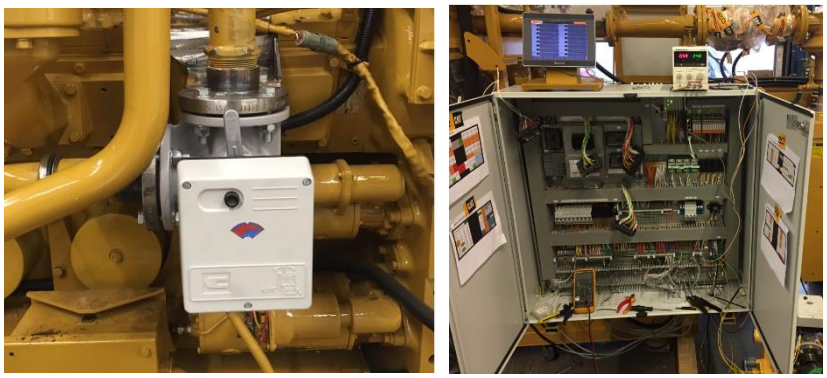

Figure 18: Cooling three-way valve with electric motor (a) and control system cabinet (b)

5.1.3 *Control systems*

(This paragraph is copied from [Bosklopper 2020b].) There are two electric control systems on the engine to allow operation on methanol. The main control system is designed and delivered by Woodward. The secondary control systems is a PLC made by PON power. Both electric systems are described as follows.

A large engine control module (LECM) is delivered and designed by Woodward to PON specification. The LECM controlled the following engine's operations: Speed/load control, Air/fuel ratio control, Air flow control, Ignition timing, injection timing control and misfire and knock detection. The LECM controlled the air throttle, methanol injectors and the spark-ignitors to perform these operations. The LECM used the air throttle and methanol injection timing for the speed/load control. Initially, the LECM will have a mapping for the injection time and ignition of every cylinder which will be adjusted during the first operations to get stable load conditions. The LECM will be also able to use the pressure sensors in the cylinder heads and control the injection timing of the individual methanol injectors for optimizing load control over the different cylinders, but this has not been tested yet and will be for future experiments.

A PLC was designed by PON Power to control all other secondary engine systems, e.g. the charged air cooling system. The PLC system is placed in a Rittal control cabinet together with the LECM as shown in figure A.1(b). This cabinet will be placed on the engine and connected to a human machine interface (HMI). The following functionalities to control and monitoring of all secondary systems are taken into the PLC: engaging/disengaging methanol fuel system, controlling manifold temperature, nitrogen inert gas system, handling of system alarm and registration of system events.

5.1.4 *Summary of most important sensors used during the spark ignited tests.*

The most important input sensors are given in

Table 4, including the range and sensitivity of these sensors. The NOx emissions are measured with the Testo-350 together with other engine emissions for further research. All sensors were calibrated prior to the testing.

Table 4: Summary of most important sensors

Sensor	Use	Range	Accuracy
In cylinder pressure sensor (Kistler 7061B)	In-cylinder pressure on cylinder 3,4,5 and 6	0 - 250 bar	± 1.25 bar
	Crank angle (CA) determination	0 - 360°	± 0.23°
TC Model TE1260	Air and exhaust gas temperatures	-40 ÷ +1000 °C	± 1.5 °C ± 0.004*(T)
PT100	Lubrication oil and cooling water temperatures	-220 ÷ +600 °C	± 0.3 °C ± 0.005*(T)
Pressure sensor 10 bar	Air and exhaust gas pressures	0 - 10 bar	± 0.02 bar
Flow sensor KRAL BEM 500	Methanol flow	0 - 300 kg/s	± 0.3 kg/s (± 0.1%)

5.2 Test plan

We performed NG performance tests for comparison with methanol performance. For NG we conducted tests at 250 kWe (50% load) and 375 kWe (75% load) with an ignition timing of 20 ^{0}CA BTDC. The engine tests on 100% methanol were performed according to a step-by-step action plan to ensure the tests were conducted safely and efficiently during the 2 weeks of testing. To get the engine running on 100% methanol, it was necessary to find the amount of methanol and air needed for stable engine operation at 0% load because this allows switching from NG to methanol at start-up in 5 seconds.

We performed the following steps to achieve the 0% stable engine load run with methanol.

- Step 1: 100% NG operation at 125 kWe
- Step 2: Slowly increasing methanol flow and decreasing NG flow at 125 kWe
- Step 3: Achieve 100% methanol at 125 kWe
- Step 4: Decrease to 0% load and determine amount of methanol and air needed at 1500 rpm.

After running the engine with 100% methanol at 0% load, stable load conditions were found for 50% and 75% load. The general operating conditions for these stable load runs are:

- Fuel injection pressure: 5 bar
- Engine speed:1500 RPM.
- Ignition moment: 20 ^{0}CA BTDC.
- End of injection was fixed between inlet valve open (IVO) and inlet valve closed (IVC). Injection ended exactly at the middle of this duration to allow all injected methanol to flow to the cylinder.
- Injection duration was load dependent varying between 5 to 25 ms.
- Constant NOx emission of 500 mg/Nm^3 at 5% reference oxygen.
- $T_{manifold}$ = 40 ^{0}C
- Air-excess ratio was varied and load dependent. Although the air-excess ratio varied, it was close to 1.60, thus, depicting lean burn engine operation.

After the stable load runs we executed a series of additional performance tests executed as shown in Table 4. The spark-timing was advanced by steps of 2 degrees, to study the impact of ignition timing sweep while keeping the NOx and load constant. We conducted this 2nd set of methanol tests at a constant NO_x emission of 500 mg/Nm^3 at 5% reference oxygen (equal to ± 340 ppm), with the main reason being the tightening emission legislations. For the NG test engine, the 500 mg/Nm^3 of NOx value is close to and lower than the NOx IMO TIER-III limit for this engine, which is 2.08 g/kWh [Sapra 2019]. We varied the air-excess ratio to keep the NOx emissions constant. The fuel pressure and engine speed were kept constant as during the stable load run conditions.

Table 5: Performance tests conducted with 100% methanol and 100% NG.

	125 kW (25 %)	250 kW (50 %)	375 kw (75 %)
Natural Gas			
20 ^{0}CA BTDC and constant NOx of 500 mg/Nm^3		X	X
Methanol			
Stable 0 % load run			
Stable load runs (at ignition timing 20 ^{0}CA BTDC) and constant NOx	X	X	X
2nd set of methanol tests (varying ignition timings)			
Ignition timing 16 ^{0}CA BTDC and constant NOx		X	X
Ignition timing 18 ^{0}CA BTDC and constant NOx		X	X
Ignition timing 20 ^{0}CA BTDC and constant NOx		X	X
Ignition timing 22 ^{0}CA BTDC and constant NOx		X	X
Ignition timing 24 ^{0}CA BTDC and constant NOx		X	X

5.3 Test results

This section discusses the experimental results and presents the impact of methanol combustion on various performance parameters such as average cylinder pressure, cycle-to-cycle variations and engine efficiency. In this analysis we compare the results for 100% methanol against those for 100% natural gas. Additionally, the section discusses the impact of variations in ignition timing on engine performance with 100% methanol. All the measurements are compared at 500 mg/Nm^3 of NOx.

5.3.1 Average cylinder pressure

We calculated the average pressure of the 60 cylinder cycles for all the four measured cylinders as function of crank angle to compare and study the in-cylinder pressures measured during 100% NG operation and 100% methanol. The engine settings corresponding to the measurements shown in Figure 19Figure 19: Mean cylinder pressure of NG compared to methanol at a power set at 375 kWe were 375 kWe power output, 500 mg/Nm^3 of NOx, ignition at 20 ^{0}CA BTDC and 1500 rpm. Figure 19 reveals that methanol showed lower in-cylinder pressures compared to NG at the same engine operating conditions. This was not the case for every single cylinder. For instance, cylinder 4 showed higher average in-cylinder pressures with methanol compared to cylinder 4 with NG. To understand the exact impact of methanol on the in-cylinder pressures further modelling and analysis should be performed.

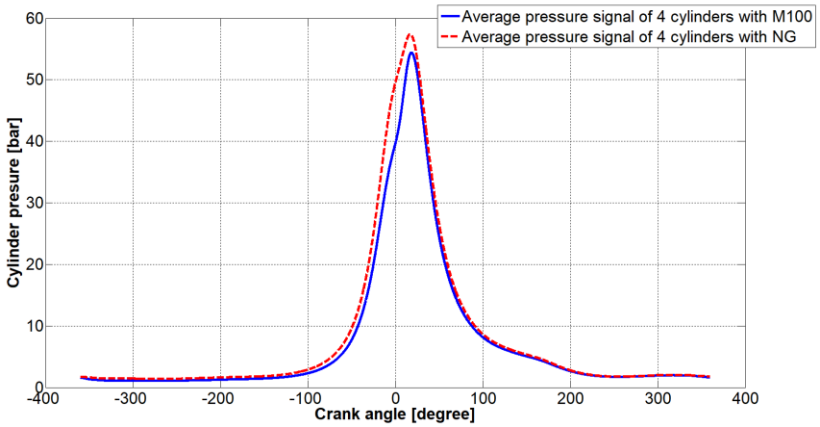

Figure 19: Mean cylinder pressure of NG compared to methanol at a power set at 375 kWe

5.3.2 *Cycle-to-cycle pressure variations*

Figure 20 shows the cyclic variations of in-cylinder pressures measured for natural gas (a) and methanol (b) at 375 kWe load, 500 mg/Nm^3 NO_x, ignition-timing of 20 ^{0}CA BTDC and 1500 rpm. To quantify the cycle-to-cycle variations and compare them for methanol and natural gas we first estimate the coefficient of variation (COV) for the maximum pressure [Xie 2013] based on 60 cycles.

$$COV_{pmax} = \frac{std_{P_{max}}}{P_{max,avg}} \cdot 100\% \quad [-] \tag{1}$$

In equation (1) $std_{P_{max}}$ is the standard deviation of the maximum in-cylinder pressure and $P_{max,avg}$ is the maximum average pressure over 60 cycles in bar.

With methanol, the COV_{pmax} varied between 9.53% and 14.82% against a variation between 7.63% and 9.34% for NG. We found higher COV_{pmax} values for all cylinders with methanol compared to NG.

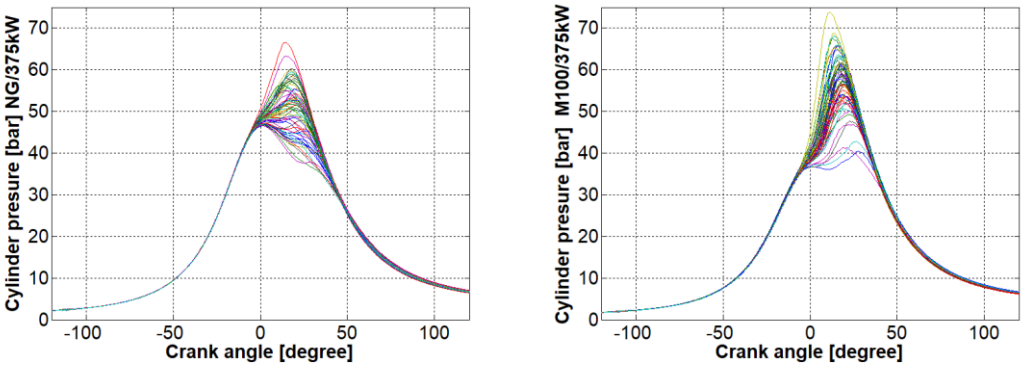

Figure 20: cycle-to-cycle pressure variation using natural gas (a) and methanol (b).

We also compared the cycle-to-cycle variations between NG and methanol by computing the coefficient of variation (COV) of the indicated mean effective pressure (imep) [Heywood 2015]:

$$COV_{imep} = \frac{std_{imep}}{imep} \cdot 100\% \quad (2)$$

Where std_{imep} is the standard deviation of the indicated mean effective pressure (imep) in bar.

The value of COV_{imep} varied between 3.72% and 6.11% for the four cylinders with in-cylinder pressure measurements at 375 kWe power and ignition timing of 20 ^{0}CA BTDC when running on 100% methanol. For NG, COV_{imep} varied between 1.76% and 2.93% at the same conditions. This is well below the 10% which is often considered the limit for stable combustion

We consider the 10% value as the misfire or stability limit. For test conditions, the values of COV_{imep} for methanol and NG were far below 10% value. However based on our measurements we find less stable engine operation with methanol than with natural gas.

5.3.3 *Impact of ignition timing variation*

Figure 21 shows the average pressure versus crank angle for various ignition timings at operating conditions of 250 kWe, 500 mg/Nm^3 NOx and 1500 rpm when operating on 100% methanol. The value of maximum pressure increased and the position shifted closer to TDC, as ignition timing was advanced from 16 to 24 ^{0}CA BTDC. Furthermore, we found indications of a higher rate of pressure rise with advanced ignition timing. Table 6 indicates no clear improvements with respect to combustion stability at different ignition timings. Compared to 100% NG operation at 250 kWe load, 500 mg/Nm^3 NOx and 20 ^{0}CA BTDC ignition timing, methanol combustion showed higher values of COV, indicating lower stability. However, the COV_{imep} values with 100% methanol never exceeded the 10% limit.

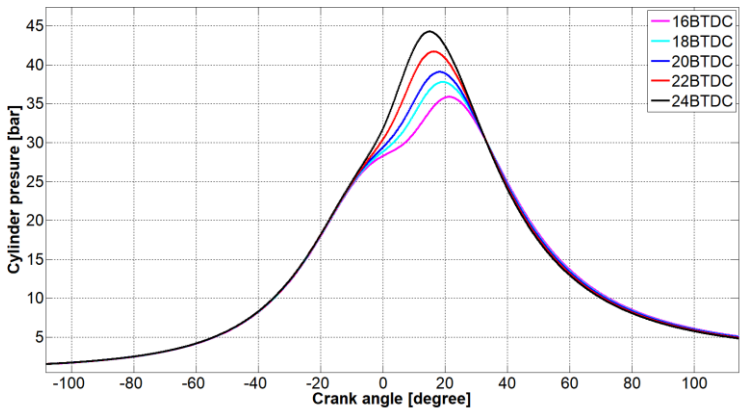

Figure 21: Mean pressure of all cylinders with changing ignition timing at 250 kWe on 100% methanol

Table 6: Average COV_{pmax} and COV_{imep} at 250 kW and 1500 rpm for methanol at different ignition timings

Ignition timing	COV_{pmax}	COV_{imep}
Ignition timing 16 ^{0}CA BTDC	12.48 %	5.02 %
Ignition timing 18 ^{0}CA BTDC	10.59 %	5.76 %
Ignition timing 20 ^{0}CA BTDC	13.09 %	4.62 %
Ignition timing 22 ^{0}CA BTDC	13.46 %	4.10 %
Ignition timing 24 ^{0}CA BTDC	12.89 %	4.55 %

5.3.4 *Aftercooler temperature variation*

We varied the temperature after the cooler, $T_{manifold}$, from 40 °C to 60 °C. This increases the in-cylinder inlet air temperature measured just before the inlet valve, $T_{inletvalve}$. This has been realized by manual closing the cooling valve to the air cooler. Increasing $T_{manifold}$ increases the fraction of fuel vaporized before entering the combustion chamber [Heywood 2105]. As the heat of vaporization of methanol is high, we expect that at higher $T_{manifold}$ more methanol will enter the cylinder in evaporated state leading to a more homogeneous mixture at ignition.

Generally a lower $T_{inletvalve}$ leads to a lower maximum in-cylinder temperature, resulting in reduced NOx emissions [Stapersma 2010b]. The trade-off between these two effects with changing $T_{manifold}$ is unknown and therefore it is important to study the impact to varying temperature settings. We varied the temperature after the cooler from 40 to 60 °C and back within a period of 20 minutes as shown in Figure 22. The methanol flow and power were kept constant on 200 kg/hr and 375 kWe.

With increasing temperature after the cooler from 40 °C to 60 °C the λ raised from 1.61 to 1.65 and the NO_x emissions dropped from 170 ppm (= 500 mg/Nm^3) to 117 ppm, which is shown in Figure 23. For other (gaseous) fuels increasing the temperature after the cooler leads to increased air / fuel temperature and consequentially raised NO_x eissions [Stapersma 2010]. However, increasing the temperature after the cooler by 20 °C, resulted not in a (trapped) in-cylinder temperature rise of 20 °C. The temperature at the inlet valve only went up from 13.5 °C to 16.0 °C, as shown in Table 7. Our assumption is that an increased manifold temperature only leads to an increase of the percentage of methanol evaporated before entering the cylinder, as the vaporization process requires a lot of input due to the high heat of evaporation of methanol.

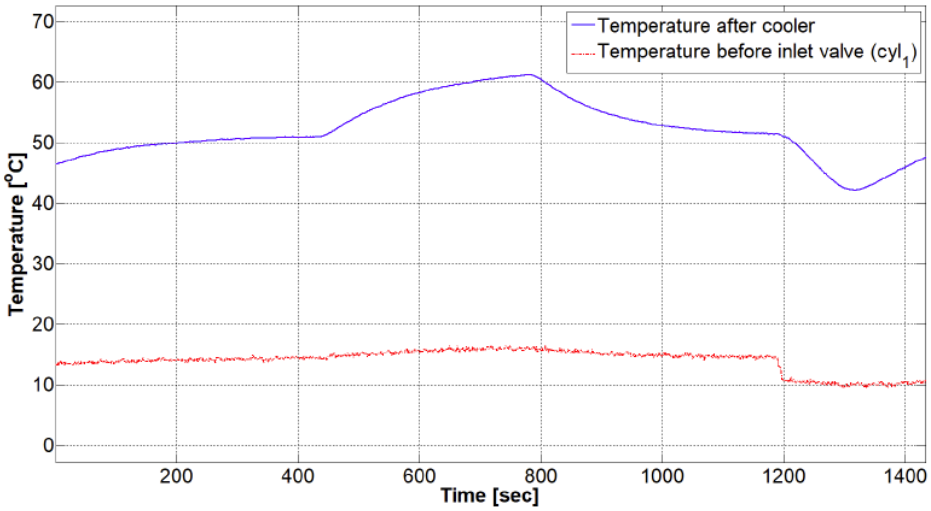

Figure 22: Variation of the aftercooler temperature and just before the inlet valve in time.

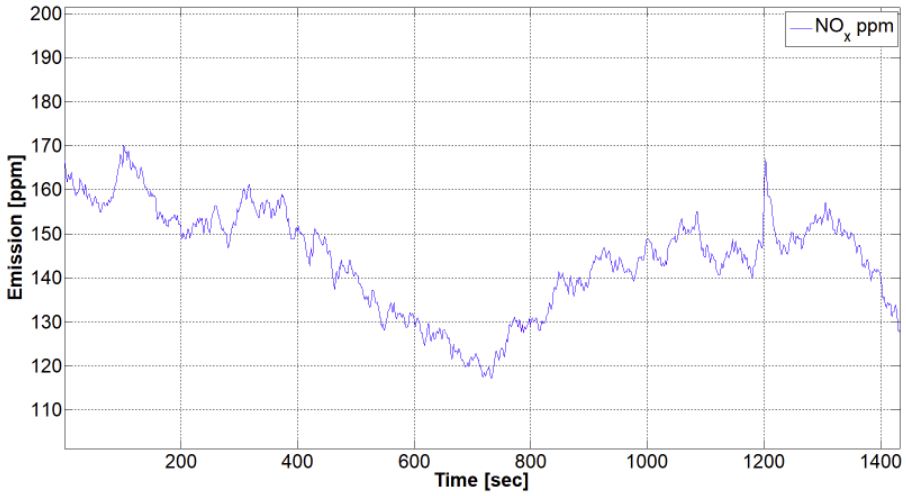

Figure 23: Nox emissions during the temperature rise to 60°

Figure 24 shows the mean in-cylinder pressure at a manifold temperature of 40 °C and 60 °C.
The figure reveals a clear difference is shown in the increasing pressure part. Where the manifold temperature is higher the pressure is increased at an earlier CA. But around 20 °CA ATDC the pressure lines cross each other resulting in a lower peak pressure with 60 °C.

Table 7: Important parameters with increasing aftercooler temperature at 375 kWe and constant fuel consumption

Tmanifold (°C)	Tinletvalve (°C)	P (bar)	λ(-)	NOx (ppm)
40	13.5	1.42	1.61	170 (=500 mg/Nm^3)
60	16.0	1.51	1.65	117 (=344 mg/Nm^3)

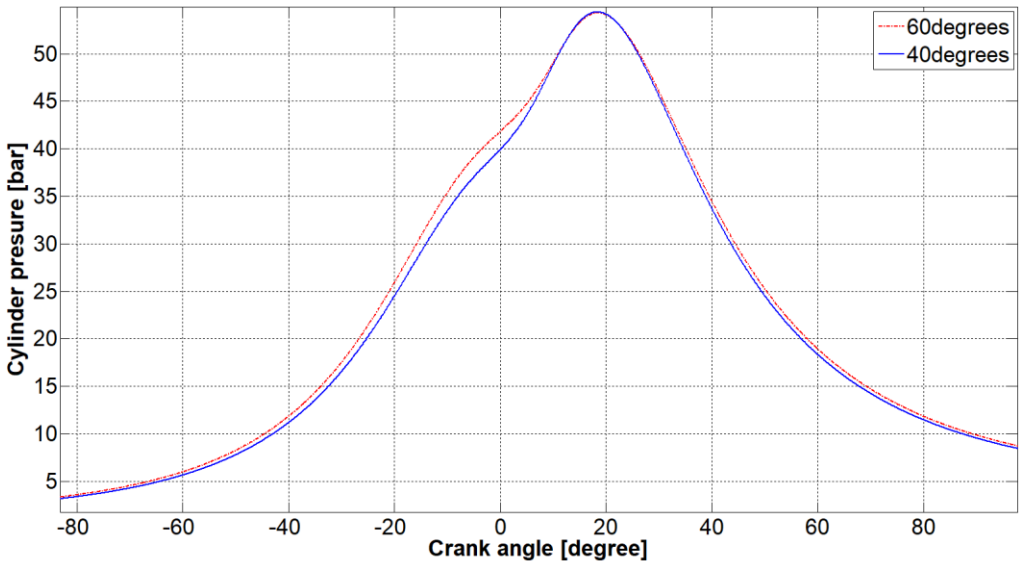

Figure 24: Mean in-cylinder pressure plots at a $T_{manifold}$ of 40 °and 60°C

5.3.5 *Combustion duration*

From the Kibox data we could calculate the crank angles at which 10%, 50% and 90% of mass fraction burned (CA10, CA50 and CA90) [Merker 2014]. We took the average value from 60 values of the four cylinders where we measured in-cylinder pressure. Table 8 shows a comparison of these averaged values for methanol with an ignition timing ranging from 16 °CA BTDC up to 24 °CA BTDC with NG with an ignition timing of 20 °CA BTDC The table shows the start of combustion (CA10), center of heat release rate (CA50), end of combustion (CA90) and combustion duration (CA10-CA90) for 375 kWe, 1500 rpm and 500 mg/nm3 NOx.

Table 8: Mean of kibox CA10 CA50 and CA90 values of the four measured cylinders with methanol with varying ignition timing compared to natural gas

	NG 20BTDC	MeOH 16BTDC	MeOH 18BTDC	MeOH 20BTDC	MeOH 22BTDC	MeOH 24BTDC
CA10	5.03	8.26	6.97	5.57	3.40	2.56
CA50	19.78	20.49	19.31	19.98	15.59	14.86
CA90	42.86	42.79	42.36	41.79	40.05	40.01
CA90-C10	37.83	34.45	35.39	36.22	36.65	37.45

Merker [Merker 2014] argues the most consumption optimal operating point of CA50 is at 8 °CA ATDC. This is almost independent of type of machine or combustion process. From table 4.6 can be seen that this optimal operating point is not obtained during the ignition variation, but with methanol at an ignition timing of 24 °CA BTDC, the CA50 value of 14,86 °CA ATDC is closest to this optimal operating point. We indeed found the highest efficiency at this ignition timing.
Table 8 also reveals a decreased combustion duration at later ignition timing. Combustion duration for methanol at 24 °CA BTDC is comparable with the combustion duration of NG at 20 °CA BTDC. In comparable settings (20 °CA BTDC) combustion duration of methanol is shorter than for NG with 1.61 °CA.

5.3.6 *Efficiency*

We encountered challenges to accurately measure NG flow during our experiments. Therefore we use an engine specific performance datasheet from the engine manufacturer with an ignition timing at 18 ^{0}CA BTDC [PON Power 1993]. The effective (brake) engine efficiency at 75 % load was 33.9 % when running on 100% natural gas (LHV = 34.5 MJ/m^3), available from Dutch NG grid. LHVs are given in Nm^3/hr for NG and kg/hr for (liquid) methanol. At 75 % engine load, NOx emissions of 500 mg/Nm^3 and ignition timing of 18 ^{0}CA BTDC engine efficiency improved to 34.8 % when operating on 100% methanol (LHV = 19.9 MJ/kg). The efficiency under equal conditions improved by 0.9 % and 2.2 % with methanol compared to natural gas at power outputs of 375 kWe and 250 kWe, respectively. Table 9 shows the engine efficiency we calculated for varying ignition angles running on 100% methanol, at an engine output of 250 kWe and 375 kWe. The maximum engine efficiency was 35.9 % with an ignition timing of 24 ^{0}CA BTDC at 375 kWe output. At the ignition timing of 18° BTDC we found an efficiency improvement of 2.2 % resp 0.9 % at an engine output of 250 kWe ans 375 kWe respectively.

Table 9: Engine efficiency at 50 and 75 % load at 500 mg/Nm^3 NOx emission

.

Test conditions	250 kWe (50 % load)	375 kWe (75 % load)
Methanol (LHV = 19.9 MJ/kg)		
Ignition timing 16 ^{0}CA BTDC	32.5%	34.4%
Ignition timing 18 ^{0}CA BTDC	33.2%	34.8%
Ignition timing 20 ^{0}CA BTDC	33.6%	35.5%
Ignition timing 22 ^{0}CA BTDC	33.8%	35.7%
Ignition timing 24 ^{0}CA BTDC	34.0%	35.9%
Natural gas (LHV = 34.5 MJ/m3)		
Ignition timing 18 ^{0}CA BTDC	31.0%	33.9%

We conclude that improvements in engine efficiency could be obtained from a retrofitted SI NG engine converted to operate on 100% methanol without making any modifications to the geometrical engine specifications such as cylinder or piston geometry. Additional efficiency improvements could be gained by optimising the engine for methanol combustion, which is recommended for future research.

Overall, the efficiency is higher compared to NG. According to Verhelst [Verhelst 2019], a higher efficiency with methanol is expected to be gained possibly due to lower wall heat losses and from the increased charge density, which leads to a higher volumetric efficiency. The impact of methanol on combustion durations and heat losses and on engine efficiency will be further studied in near future by developing in-cylinder heat-release models.

5.3.7 *Top dead center Shift*

In our measurement setup, we do not have a direct measurement of the moment the cylinder is at top dead center. Before starting the experiments we correlate the pressure signal to the Crank Angle. This calibration process takes place before the

experiments and we have to account for a possible shift of this position during the experiments. The calculations of indicated power, but also of the reaction coordinate (a measure of the amount of fuel burned at a certain moment in time) is highly sensitive for this calibration process. Figure 25 shows the pressure signal for three TDC shifts.

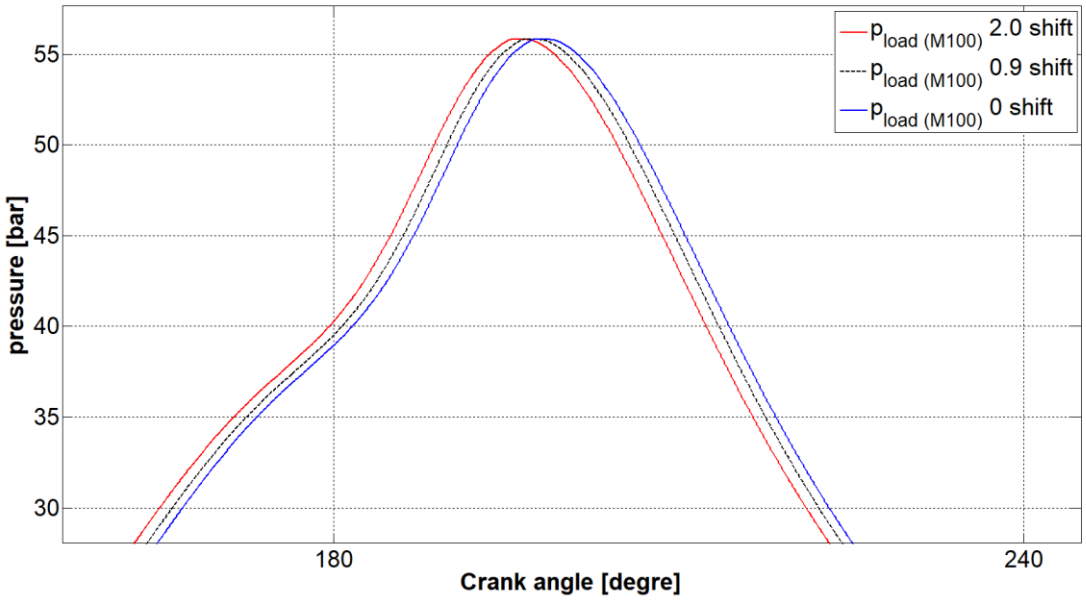

Figure 25: Pressure signal of methanol with three TDC shifts

We made two assumptions to determine the TDC from measured brake power:

- We assume that the mechanical efficiency is constant, at 91%, which is stated as nominal value for a diesel engine. We assume that for NG and methanol the mechanical efficiency remains the same and does not change depending on the fuel.
- We assume that the engine power is equally divided over 8 cylinders cylinders

Then, with the known brake power, an indicated power per cylinder can be calculated. The indicated power calculated from the brake power equals the indicated power calculated from the pressure signal at a TDC shift of -0.9° CA. This TDC shift is applied in all calculations on the NG model.

5.4 Modelling

The used model is described by [Sapra 2020b]. The engine and engine data is described in detail by H. Sapra. The specifications of the engine are given in Table 3 and are similar to the values in the model files of the engine. The model of H. Sapra has been used for the modelling of the engine with NG. Boskoppler applied a few modification to the model of Sapra:

- Bosklopper added a heat loss to crevices submodel in the model of Harsh Sapra, although he did not use this submodel in his calculations.
- The IVO is slightly changed to 353,3 CA.
- The induced temperature (T_{ind}) in the T_1 formula is not calculated with $T_{manifold}$, but with $T_{inletvalve}$, because an extra temperature sensor is placed during these experiments in the

inlet valve. Reason for this is that an additional sensor was placed in the inlet valve and this sensor is closer to the in-cylinder temperature.

5.4.1 *The in-cylinder Heat release (HR) model*

The heat release calculation model is normally used to calculate temperature and heat release rate (HRR) is shown in Figure 26. This model requires cylinder pressure and the crank-angle (α) as the input [Stapersma 2003; Ding 2011]. In the project we measured both pressure and crank angle α with the Kibox. All sub-models of the model up to the point that the HRR can be calculated are discussed in [Bosklopper 2020a]. A block diagram of the whole process is given in Figure 27 leading to CRR and ξ. All formulas used by Bosklopper are from Stapersma [Stapersma 2010c. Stapersma 2010d and Stapersma 2010e].

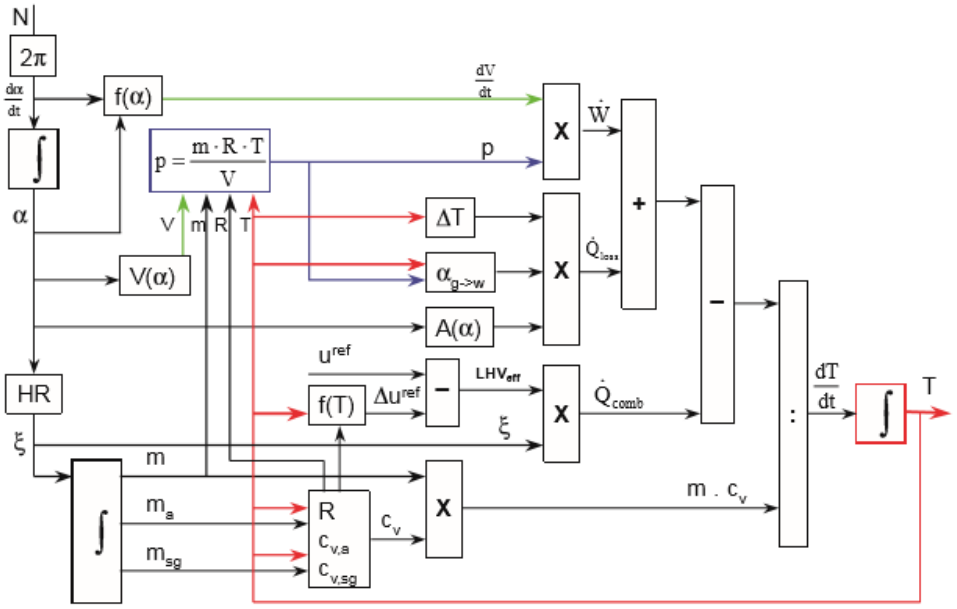

Figure 26: Block diagram of the Heat release calculation model resulting in in-cylinder temperature [Stapersma 2003; Ding 2011]

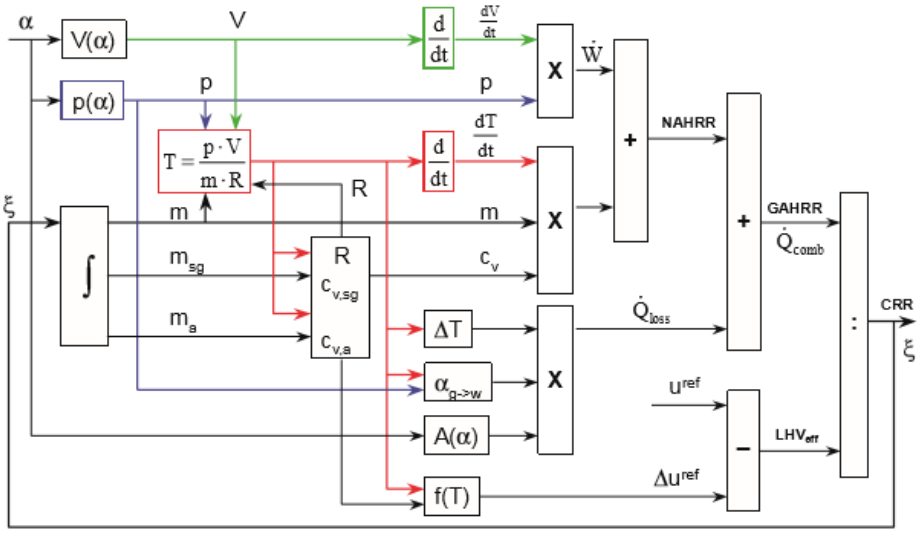

Figure 27: Block diagram of the Heat release calculation model [Stapersma 2003; Ding 2011]

The model relates the crank angle to the in cylinder volume using the engine specific geometries crank radius, rod length, cylinder bore and minimum cylinder volume. With use of the ideal gas law, the model calculates the in cylinder temperature.
The model estimates the air excess ratio using the measured molfraction of oxygen in the exhaust gas. from the exhaust gas. A second way to estimate the air excess ratio is by measuring the CO_2 emissions in the exhaust gas. The air excess ratio was 1,69 for the method using oxygen and 1,63 for the method using CO_2.
For this specific engine, the trapped air mass estimation is quite complicated. This particular engine has zero valve overlap to avoid methane slip. As result the exact trapped mass is not exactly known. The trapped mass consists of two fractions: the fresh mass and the residual gas from the previous cycle. The fresh mass, consisting of the freshly added air and the fresh fuel, can be determined from measurements. Harsh Sapra [Sapra 2020] calculated the residual mass to be about 15 % of the total mass in the cylinder.
As the engine has no scavenge period, the temperature in the cylinder at the moment inlet valve closes is calculated using formula (3) and (4)

$$T_{bld} = \left(\frac{P_{bld}}{P_{EO}}\right)^{\frac{n_e-1}{n_e}} = \left(\frac{P_{bld}}{P_{EO}}\right)^{\frac{0.3}{1.3}} \quad (3)$$

$$T_1 = \frac{1}{\frac{V_{IC}-V_{IO}}{V_{IC}\cdot T_{ind}} + \frac{V_{EC}\cdot P_{bld}}{V_{IC}\cdot P_t \cdot T_{bld}}} \quad (4)$$

With:

T_{ind} = measured temperature before inlet	[K]
V_{IC} = Cylinder Volume at Inlet Closing	[m^3]
V_{IO} = Cylinder temperature at inlet opening	[m^3]
V_{EC} = Cylinder volume at exhaust valve closing	[m^3]
P_{bld} = Blowdown pressure (the pressure at exhaust valve opening)	[N m^{-2}]
P_t = turbo pressure (measured)	[N m^{-2}]
T_{bld} = Blow down temperature	[K]
P_{EO} = pressure at exhaust valve opens	[N m^{-2}]

The heat of combustion equals the product of combustion rate and internal energy change resulting from the combustion. The heat loss is modeled using the Woschni model with coefficients adapted for this engine as determined by Sapra [Sapra 2020].
Now the net apparent heat release rate (NAHRR) can be calculated using

$$NAHRR = \dot{Q}_{combustion} - \dot{Q}_{loss} + \dot{E}_{fuel} = m \cdot C_v \cdot \frac{dT}{dt} + p \cdot \frac{dV}{dt} \quad (5)$$

With:

$$\dot{E}_{fuel} = \dot{m}_{fuel} \cdot \left(h_{fuel,liquid} - u_{fuel,gas}\right) \quad (6)$$

The gross apparent heat release rate (GAHRR) can be calculated with:

$$GAHRR = \dot{Q}_{combustion} + \dot{E}_{fuel} \quad (7)$$

Finally the combustion reaction rate (CRR) can be calculated using

$$CRR = \xi = \frac{m \cdot C_v \cdot \frac{dT}{dt} + p\frac{dV}{dt} + \dot{Q}_{loss}}{u_{combustion} + e_f}[-] \quad (8)$$

With

$NAHRR$	= Net apparent heat release	[kJ s^{-1}]
$\dot{Q}_{combustion}$	= Heat flow resulting from fuel combustion	[kJ s^{-1}]
$\dot{Q}_{loss}$	= Heat loss through cylinder walls etc	[kJ s^{-1}]
$\dot{E}_{fuel}$	= Heat flow to the fuel for evaporation	[kJ s^{-1}]
M	= mass	[kg]
C_v	= specific heat (constant volume)	[kJ $kg^{-1}K^{-1}$]
T	= Temperature	[K]
t	= time	[s]
$\dot{m}_{fuel}$	= mass flow fuel	[kg s^{-1}]
$h_{fuel,liquid}$	= enthalpy of the liquid fuel	[kJ kg^{-1}]
$u_{fuel,gas}$	= internal energy of gaseous fuel	[kJ kg^{-1}]
e_f	= energy to heat up and evaporate the fuel	[kJ kg^{-1}]
$u_{combustion}$	= heat released during fuel combustion	[kJ kg^{-1}]

The integral of CRR to the time is the Reaction Coordinate (RCO). The RCO varies from zero at inlet valve closes; becomes slightly negative as result of evaporation process and heat losses, and should rise up to 1 if all fuel is burned. The RCO is used in paragraph 5.3.5 to estimate combustion duration.

5.4.2 Methanol as fuel

Bosklopper modified two files in them odel of Saprah: the gas properties file and the fuel properties file.

The ”gas properties” parameter file describes the energy of every component in the combustion chamber. The total enthalpy of the entering fuel and the internal energy of the gaseous fuel are needed from methanol. Both enthalpy and internal energy are dependent on temperature.

The ”fuel properties” parameter file describes all other needed properties for methanol, which are needed in the model such as fuel density, temperature at injection and the fuel specification in molecular mass.

5.4.3 Heat loss to liquid fuel

Equation (6) describes the energy balance of the fuel in the model:

$\dot{E}_{fuel} = \dot{m}_{fuel} \cdot (h_{fuel,liquid} - u_{fuel,gas})$.

The original model assumes that the fuel is injected as liquid in the combustion chamber and evaporates immediately (injection rate and evaporation rate are equal. Figure 28shows schematically the processes in the in-cylinder model. Energy flows from the control volume to the fuel. This energy flow is indicated as $\dot{Q}_{loss,fuel}$. This is the energy required to heat up and evaporate the fuel. This energy flow was removed by Sapra as the gas entered the cylinder in liquid form.

Bosklopper placed this sub model back with two modifications. He added a submodel to calculate the heat added to the methanol in the manifold. This heat is used to evaporate part of the methanol. The second modification is that, based on the heat balance in the manifold and the temperature at the inlet valve, a percentage of the methanol enters the combustion chamber as fluid, and the remainder enters as gas.

Bosklopper made the following assumptions:

- The process is adiabatic. The heat transfer from/to the walls is zero.
- Phase transition is much faster than the vapor transport into the cylinder.
- The process is in steady state (therefore, accumulation = 0).
- There is no change in flow speed, therefore change in kinetic energy is assumed 0.

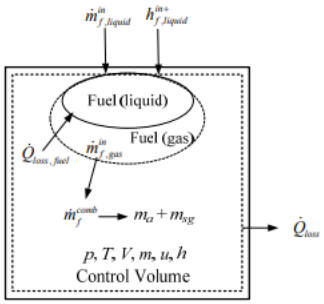

Figure 28: Schematic representation of the processes in the control volume of the in-cylinder model

5.5 Model Analyses

5.5.1 Pressure

Figure 29 shows the pressure variation in cylinder 4. Pressure rises earlier when using Natural gas, but the peak pressure is significantly lower. Also pressure increases more rapidly after TDC when injecting methanol, compared to natural gas.

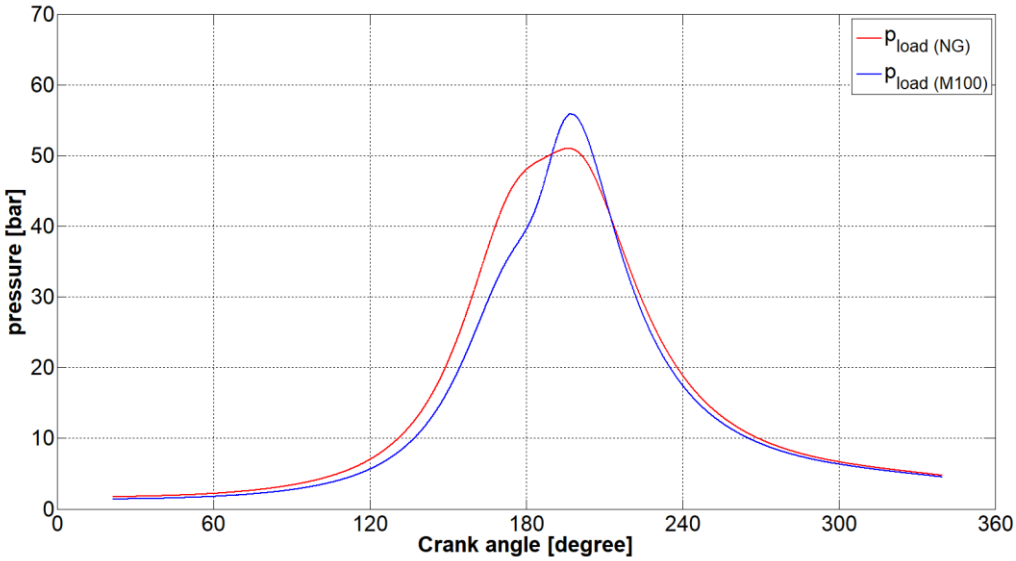

Figure 29: pressure in cylinder 4 for NG and methanol at an engine output of 375 kWe, and an ignition timing of 20 CA BTDC

5.5.2 *Ignition timing*

Figure 30 shows the average pressure variation in cylinder 4 with changing ignition timings. The maximum pressure increases and the position shifts closer to TDC, as ignition timing advances from 16 to 24 °CA BTDC. The figure also indicates a higher rate of pressure rise with advanced ignition timing. Table 9 also reveals an increased efficiency with advanced ignition timing, correlated to a maximum pressure closer to TDC.

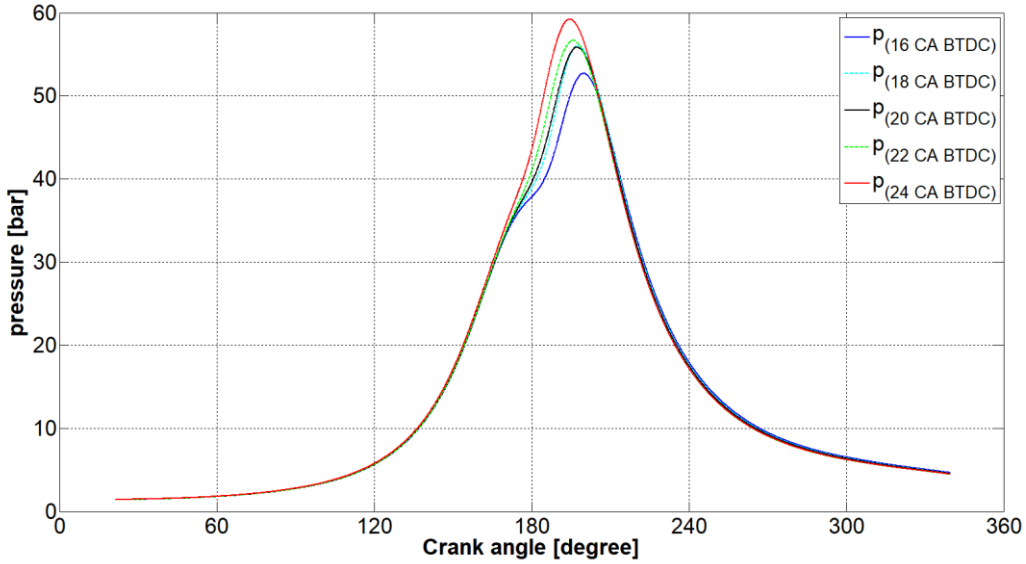

Figure 30: Pressure plot of cylinder 4 for methanol at 375 kWe with varying ignition timing

5.5.3 *Aftercooler pressure variation*

Figure 31 shows the pressure for the model of cylinder 4 with varying manifold temperature. The figure indicates an increased pressure at earlier CA correlated to an elevated manifold temperature Around 20 °CA ATDC the pressure lines cross each other and peak pressure is reduced when manifold temperature equals 60 °C.

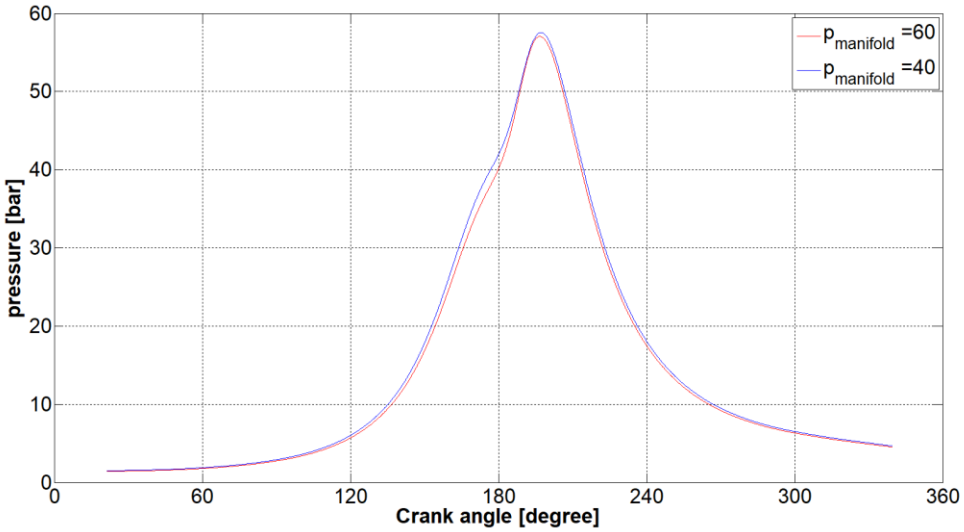

Figure 31: Pressure plot of cylinder 4 with varying manifold temperature at 375 kWe at an ignition timing of 20 °CA BTDC

5.5.4 *Indicated power vs crank angle*

Figure 32 shows the indicated power vs crank angle for Natural gas compared to Methanol. At comparable settings the maximum power is reached at earlier CA for Methanol compared to natural gas. The negative power during the compression stroke is lower for methanol. This is the result of lower in-cylinder pressure at inlet valve closing. This lower negative power has a positive influence on the efficiency of the engine.

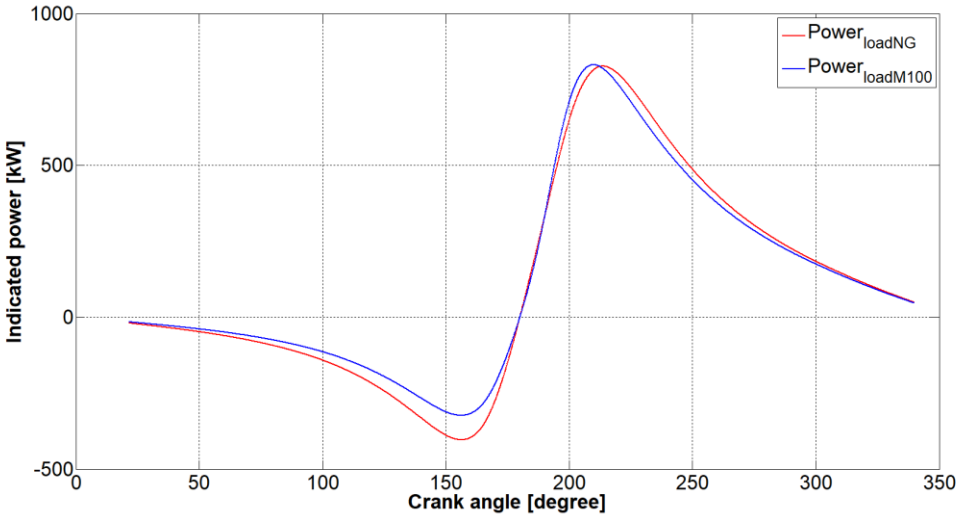

Figure 32: Indicated power plot of cylinder 4 for NG compared to methanol at 375 kWe

Figure 33 shows the indicated power vs crank angle for different ignition timings for cylinder 4. The calculated mean indicated power varied between 52,41 kW (at 24 CA BTDC), 53,26 kW (at 20 CA BTDC) and 53,96 kW (at 16 CA BTDC) at changing ignition timings with 375 kWe power. With advanced ignition timings the maximum power is reached at earlier CA. We may expect a small variation of mechanical efficiency with varying pressure vs crank angle as the efficiency of transfer of energy from a translational motion at the cylinder head to a rotational motion at the crank is impacted by the pressure vs crank angle signal.

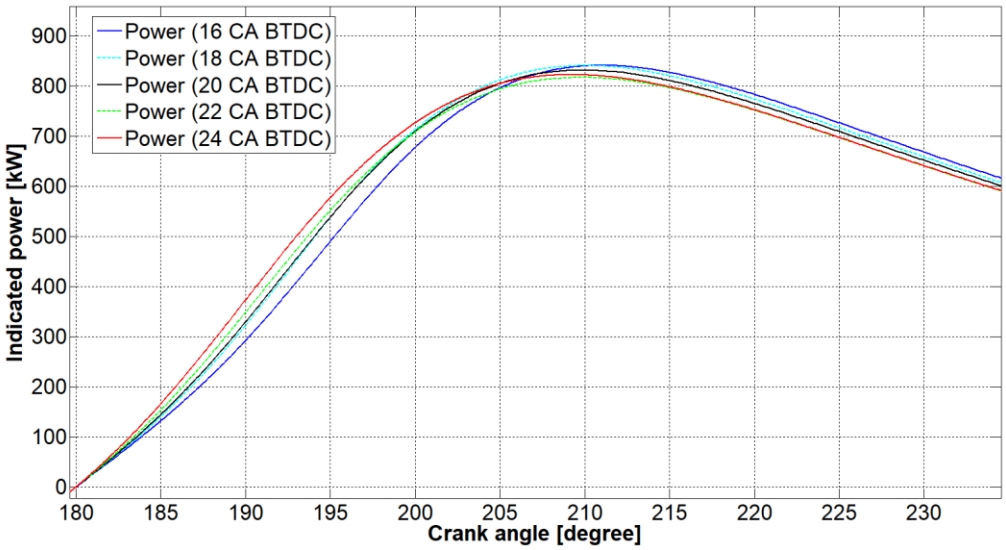

Figure 33: Indicated power plot of cylinder 4 at varying ignition timing

5.5.5 *Heat release*

Bosklopper discusses the heat release flow graphs and fuel burnt (RCO) graphs for the NG compared to methanol, the ignition variation and the temperature variation. For comparison with NG and the ignition variation he also analysed combustion duration. Furthermore we discuss the start of combustion and end of combustion for varying ignition timing. The model assumes the end of RCO is assumed at 98%. This means that at the end the in-cylinder cycle 98% of the fuel is burned.

Literature study reveals several options how the heat release should look like. All literature acknowledges four different phases in a heat release curve are: ignition delay, premixed combustion, diffusive combustion and late combustion. In our analyses we encountered a clearly visible dip in the curves, that we attribute to fuel vaporization. This dip is more pronounced for methanol, because methanol has almost 4 times the heat of vaporization compared to diesel.

NG compared to methanol

Figure 34 shows the calculated Heat release rate of natural gas compared to methanol at 375 kWe. Maximum heat release takes place earlier after TDC for methanol than for natural gas. This is an indication of faster combustion during the premixed combustion phase.

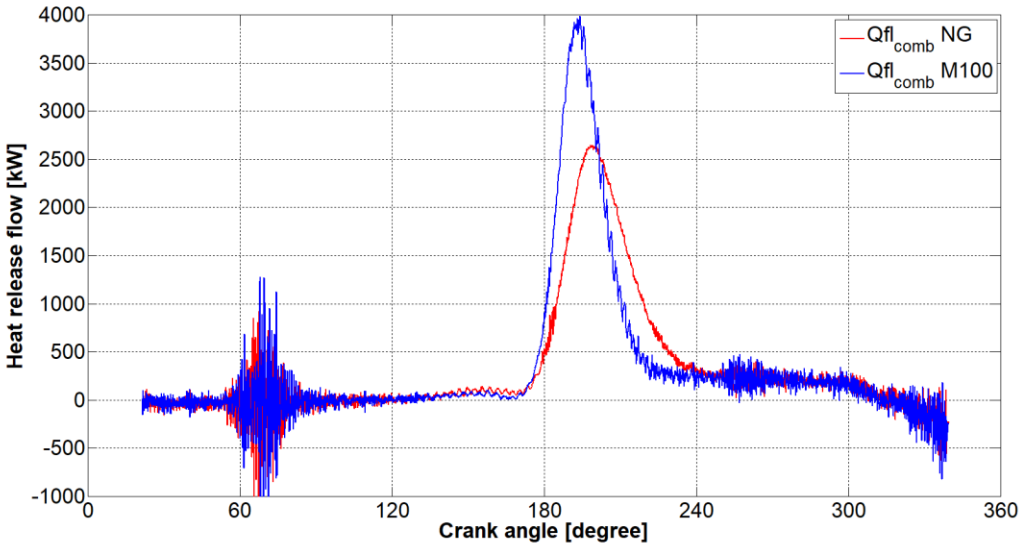

Figure 34: HRR plot of cylinder 4 with NG and Methanol at 375 kWe both at an ignition timing of 20 CA BTDC

Figure 35 shows the RCO plot of Methanol compared to natural gas. It is clearly visible that 10 % and 50 % are reached earlier for methanol. The 90 % is reached at comparable crank angle.

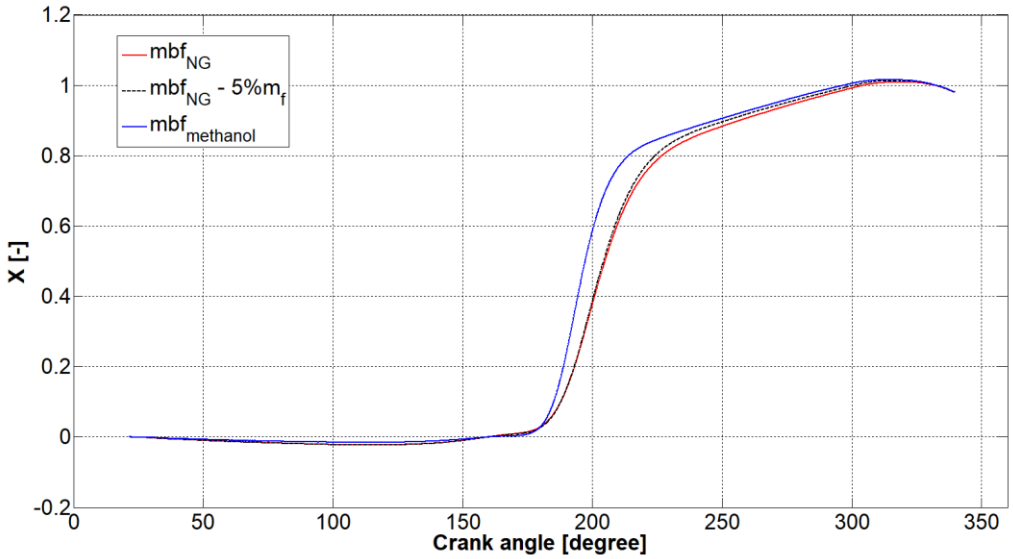

Figure 35: RCO plot of cylinder 4 with NG and methanol at 375 kWe both at an ignition timing of 20 CA BTDC

Ignition variation

Figure 36 shows the RCO plot for varying ignition timings. The plot focuses on start of ignition. We define start of ignition at the moment RCO equals 0 again. This is the moment when the heat of combustion equals the heat requirement of vaporization. With an ignition timing retarded to 16 CA BTDC we found the curve to decrease below 0 again after the defined start of combustion. This indicates that during 5 crank angles, the calculated heat release from combustion was lower than the combined heat loss to the walls and heat required for evaporation.

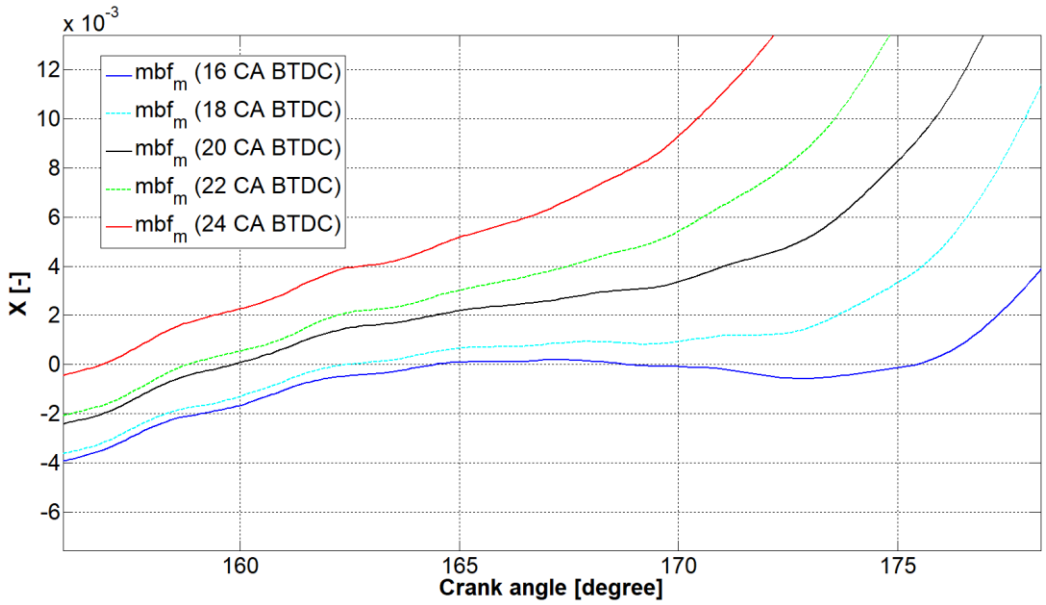

Figure 36: RCO plot focusing on the start of ignition for varying ignition timing

Bosklopper, in his thesis also shows the total RCO vs crank angle plot. Besides the varying RCO vs crank angle, which during the first combustion phases do not reveal anything strange, it appears that, irrespective of the start of combustion, 75% of the fuel is burned at around the same crank angle.

In all plots, we found a calculated RCO slightly above 100 %, which could be an indication of over estimation of the heat loss to the cylinder walls, head and the piston (the Woschni parameters).

5.5.6 *In cylinder temperature*

The in cylinder temperature is calculated with the ideal gas law in the analysis of Bosklopper. He first compared the temperature of methanol compared to natural gas (Figure 37). The figure reveals a faster increase of temperature for methanol compared to NG, which indicates faster combustion for methanol compared to natural gas under equal conditions. The steeper temperature rise, which is a function for the measured pressure, impacts the calculated combustion duration and the heat release.

After the maximum temperature is reached both curves look similar but shifted. At equal crank angle, temperature for methanol is lower, which has a positive impact on heat losses and on emissions of for instance NOx.

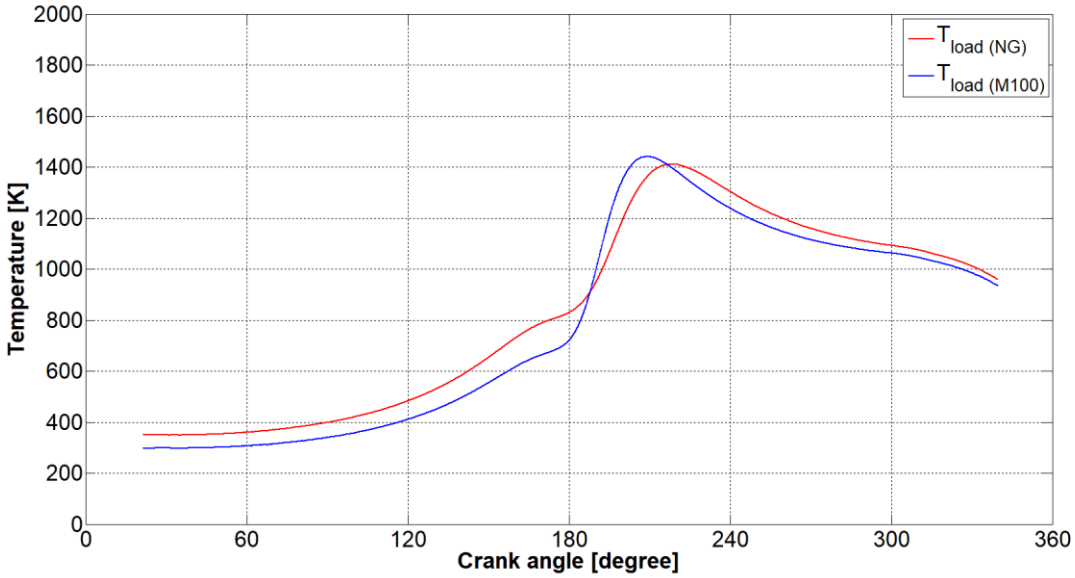

Figure 37: Temperature plot of cylinder 4 with NG vs M100 at 375kWe

In his thesis, Bosklopper also discusses the impact of ignition variation. He found both a shift to later crank angles with later ignition timing, and higher peak temperatures.

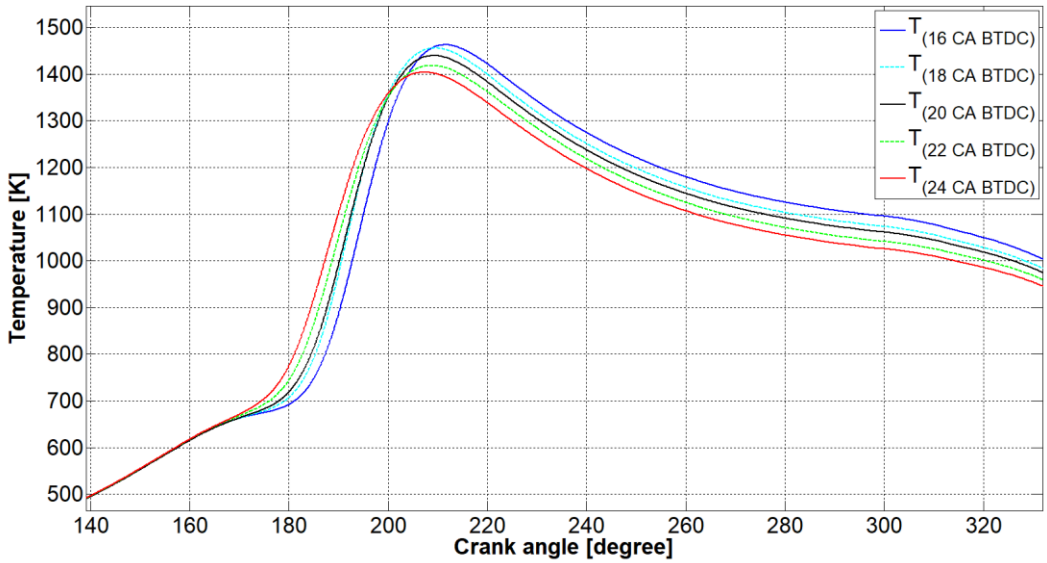

Figure 38: Temperature plot of cylinder 4 with changing ignition timing at 375 kWe

5.5.7 *Efficiency*

With the model, Bosklopper calculated the indicated efficiency and compared natural gas with methanol, as well as the different ignition timings. The indicated efficiency for methanol was, at 37.7 %, 1.2 % higher than for natural gas under the same conditions. Bosklopper also found higher efficiencies for advanced ignition timing.

5.6 Conclusions

We could conclude the following from the tests on the spark ignited engine:

- The engine runs stable on 100% methanol at 250 kWe (50% load) and 375 kWe (75% load) between 16 ^{0}CA BTDC and 24 ^{0}CA BTDC ignition timing at 500 mg/Nm^3 NOx emission.
- The experiments showed higher COV_{imep} for methanol compared to natural gas at all tested conditions, indicating lower stability. Our hypothesis is that the higher cyclic variations are due to one or a combination of following reasons: a.) Blocked injectors, b.) High evaporation heat of methanol and c.) Lower flame speed of methanol at the tested leaner air-excess ratios.
- Methanol shows 7.0 °CA's earlier CA50 and 2.6 °CA's earlier CA10 compared to NG. Indicating faster (premixed) combustion. But due to late CA90, the combustion duration is almost equal
- A changing temperature after the cooler did not lead to significant changes calculated in the CA10, CA50, CA90 and the combustion duration
- Methanol shows steeper increase of pressure after TDC compared to NG, indicating faster combustion after TDC.
- The maximum pressure increased and the position shifted closer to TDC, as ignition timing was advanced from 16 to 24 °CA BTDC, leading to engine efficiency improvements
- Maximum in-cylinder temperatures around 1400 K were reached for NG and methanol, as expected due to fixed NOx emission settings with both measurements. Only with methanol maximum temperature was reached about 20 CA earlier.
- Maximum temperatures at an earlier CA results in a lower (in-cylinder) exhaust temperature. Methanol also has lower exhaust temperatures compared to NG, and with the ignition variation at an advanced ignition timing of 24 °CA BTDC.
- Efficiency improved by 0.9% and 2.2% with methanol compared to natural gas at same test conditions of power output, ignition timing and NOx emissions. These preliminary methanol engine results show that improvements in engine efficiency could be obtained from a retrofitted SI NG engine converted to operate on 100% methanol without making any modifications to the geometrical engine specifications such as cylinder or piston geometry.
- The maximum pressure increased and shifted closer to TDC with advanced ignition timing when operating on 100% methanol. Thus, leading to engine efficiency improvements of about 1.5% at advanced ignition timing of 24 ^{0}CA BTDC compared to 18 ^{0}CA BTDC.

- A decrease of 21 °C in maximum in-cylinder temperatures calculated at an increase of manifold temperature from 40 to 60 °C, at equal power output and equal fuel consumption. Lower in-cylinder temperatures are expected to relate to lower measured NOx emissions.
- We assume that increasing the manifold temperature further improves in-cylinder performance until 100% vapor is reached at the moment of IVC.

6 Direct injection of a methanol-pilot fuel mixture in a compression ignited Internal Combustion Engine (ICE)

For this study we used a compression ignited engine, where a methanol-diesel mixture is directly in the cylinder, and ignited by compression. Figure 12 shows how the process works in this engine. Figure 39 shows the MAN 4L20/27 test engine in the lab facilities in building 'Medemblik' in Den Helder. Table 10 gives the main parameters of the engine. Diesel is injected directly in the cylinder using a plunger pump.

6.1 The MAN 4L20/27 4 stroke compression ignited engine

Figure 12 shows how the process works in this engine. Figure 39 shows the MAN 4L20/27 test engine in the lab facilities in building 'Medemblik'in Den Helder. Table 10 gives the main parameters of the engine. Diesel is injected directly in the cylinder using a plunger pump.

Figure 39: The diesel engine is a MAN 4L20/27 4-stroke Compression Ignited Diesel Engine

Table 10: Main parameters of the MAN 4L20/27 4-stroke Compression Ignited Diesel engine

Parameter	Variable	Value
Engine		MAN 4L20/27
Stroke	(L_S)	0.27 [m]
Bore	(D_B)	0.20 [m]
Number of cylinders	(i)	4 [-]
Nominal Power	(P_b)	340 [kW]
Nominal Torque	(M_b)	3247 [Nm]
Connecting rod	(CR)	0.52 [m]
Start of Injection	(SI)	4 [degree bTDC
Inlet valve Closes	(IC)	20 [degree aBDC]
Exhaust valve Opens	(EO)	300 [degree aBDC]
Nominal speed	(N)	1000 [rpm]

6.1.1 Modifications for safe operation with methanol

Safety

Methanol requires several precaution measures, part of which is determined by toxicity for primates. Table 11 lists the toxicity parameters of methanol. In consultation with the risk manager we took measures for personal protection and for fire protection. The measures consisted of wearing a full face mask with AX filter, protective clothes (gloves, shoes and overall) when handling methanol. Before entering the pump room or engine room we checked the methanol content in the air from outside the rooms. We installed thermal UV/IR cameras to monitor the rooms on unexpected heat as flames from a methanol fire are invisible to the human eye.

Table 11: toxicity parameters methanol

Flammable
Oral toxic
Dermal toxic
Inhalation toxicity
Special organ toxicity by single exposure

Fuel system

Figure 40 shows the schematic setup of the fuel system. Methanol is supplied to the inox mix tank which is specially constructed for these tests. The amount of methanol is measured using a balance on which the tank is mounted. After that F76 is supplied to the tank from the daily supply tank until the desired ratio methanol – F76 is reached. During filling and during testing the mixture is stirred continuously. We regularly checked the mixture by taking samples from the tank. All installed piping was double walled INOX piping up to the engine.

Fuel flow is measured using a Coriolis meter described in the appendix.

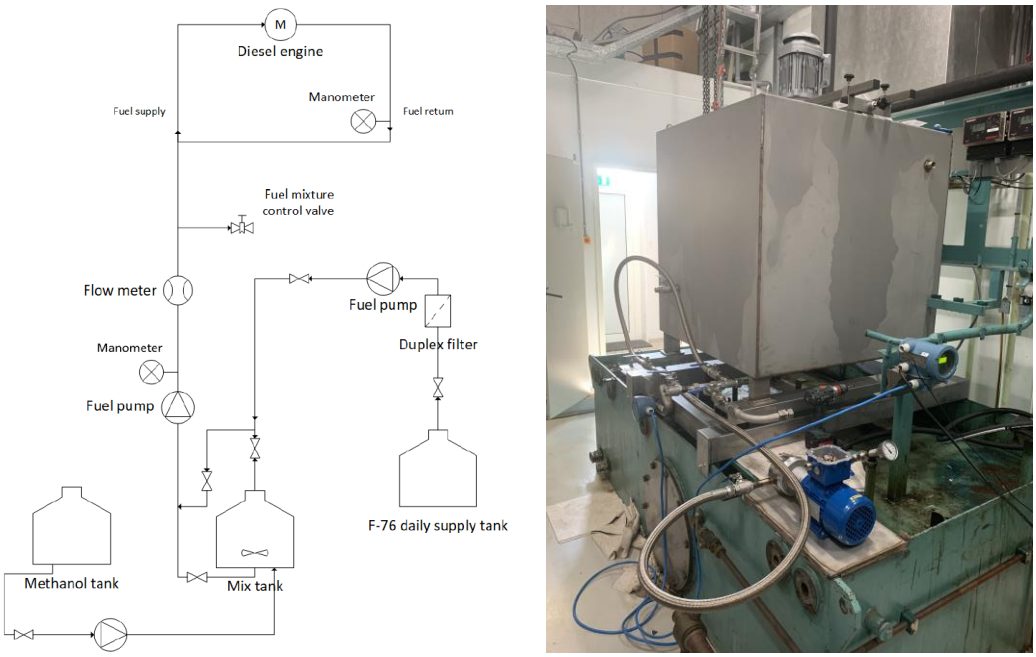

Figure 40: Modified fuel system: lay-out (left) and mix tank with stirring device mounted on the scale (right)

6.2 Test plan

Tol used three different methanol / diesel blends. He first performed measurement with 100 % diesel. Then he added methanol up to the moment that 10 % of the energy was supplied by methanol (further referred to as M_{10}). The third mixture contained about 37,5 % volumetric of methanol, so 20 % of the energy was supplied by methanol (referred to as M_{20}). For each blend he followed the measurement grid shown in Figure 41.

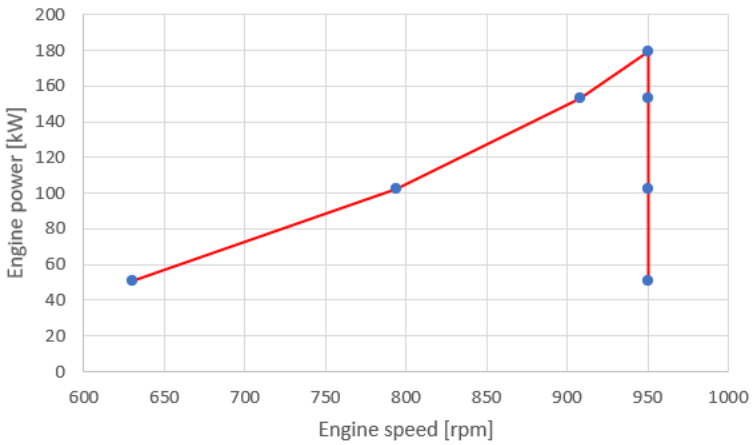

Figure 41: Measurement grid for each fuel blend

6.3 Test results

6.3.1 *Top dead center shift*

Just as in the tests performed by Bosklopper Tol used the Kibox to measure the pressure signal as function of crank angle. Also Tol had to shift the Top dead center in the software to correctly correlate the pressure signal to the crank angle. Tol used the IC angle, which is 160° BTDC for the MAN 4L20/27. In the pressure signal, IC was found at 167° BTDC, so Tol applied a TDC shift of 7° CA.

6.3.2 *Cylinder pressure measurement*

Figure 42 shows a typical pressure signal as we measure it (in this case the engine is running on F76). The pressure signal show a heavy variation at high in-cylinder pressures. This variation is known to be an artefact of the lay-out of the pressure sensors in this engine. The sensor is located in an tube connected to the cylinder. Pressure fluctuations and air flow in the tube cause the sensor to detect pressure fluctuations at a frequency equal to the Helmholtz frequency.

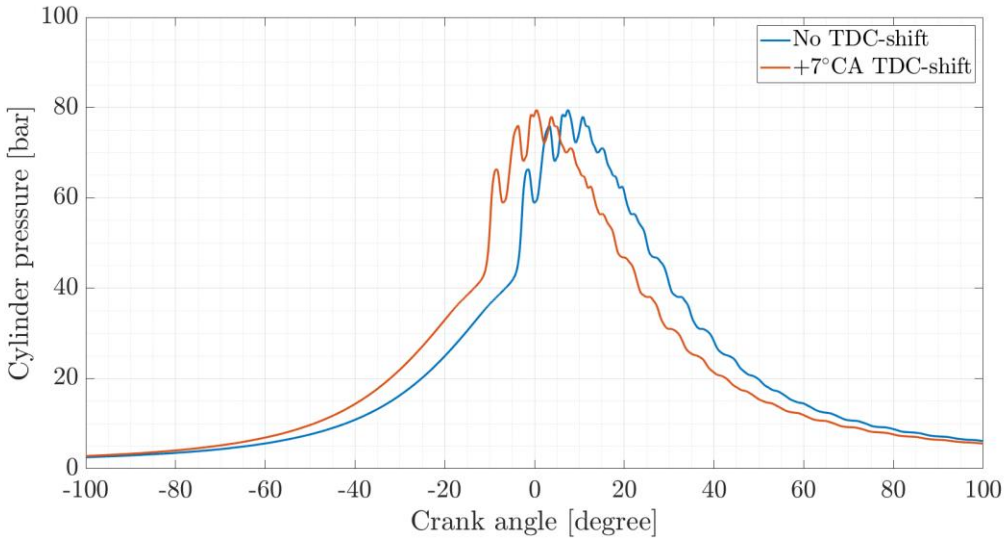

Figure 42: Pressure signal with and without TDC shift

As these fluctuations are known to be an artefact, Tol smoothed the pressure signals using the CurveFittingToolbox from MATLAB 9the unfiltered data are of course still available). The resulting signal is represented in a way that the Helmholtz frequency is filtered out. By smoothing a signal, it is possible that some information from the signal is filtered out. Figure 42 shows a typical resulting smoothed pressure signal such as is used in the further analysis.

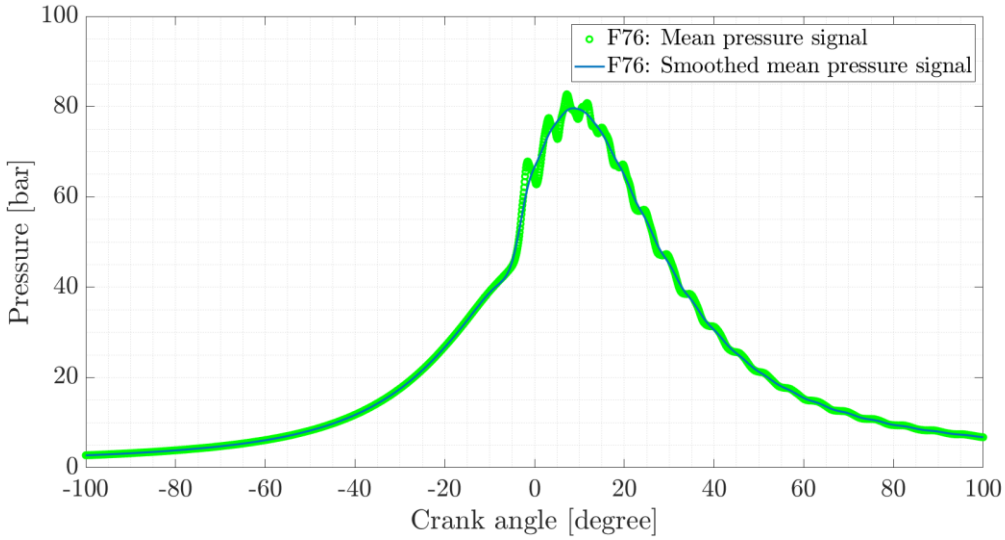

Figure 43: Smoothed pressure signal (F76)

6.3.3 *Pressure analysis*

The pressure signals we discuss are each time the average over 41 cyclles. The measurements tables consist of a data point each 0.1 degree crank angle. Figure 44 shows the pressure signal for M20, measured at an engine output of 190 kW at 950 rpm. Cylinder 1 has a different

fuel injector and cylinder head which affects the combustion. In his thesis Tol discussed the signal of cylinder 1 separate from the other pressure signals.

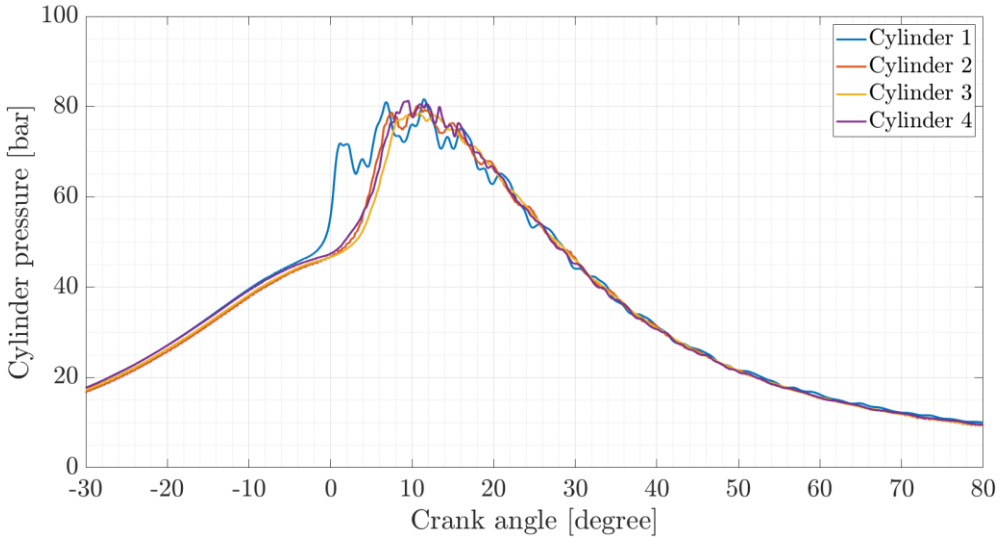

Figure 44: In-Cylinder mean pressure (averaged over 41 cycles) signals of 4 cylinders at 950 rpm and 180 kW

6.3.4 *Cycle-to-cycle pressure variations*

Tol performed analysis to study the pressure variations in the same way as Bosklopper. The only difference is in the number of cycles: Bosklopper used 60 cycles, where Tol used 41 cycles. Figure 45 reveals an increase of COV $\underline{P_{max}}$ with increase of methanol content, but the COV stayed well within the 10 % limit. The COV IMEP generally showed an increasing trent, except for cylinders 3 and 4 running on M20.

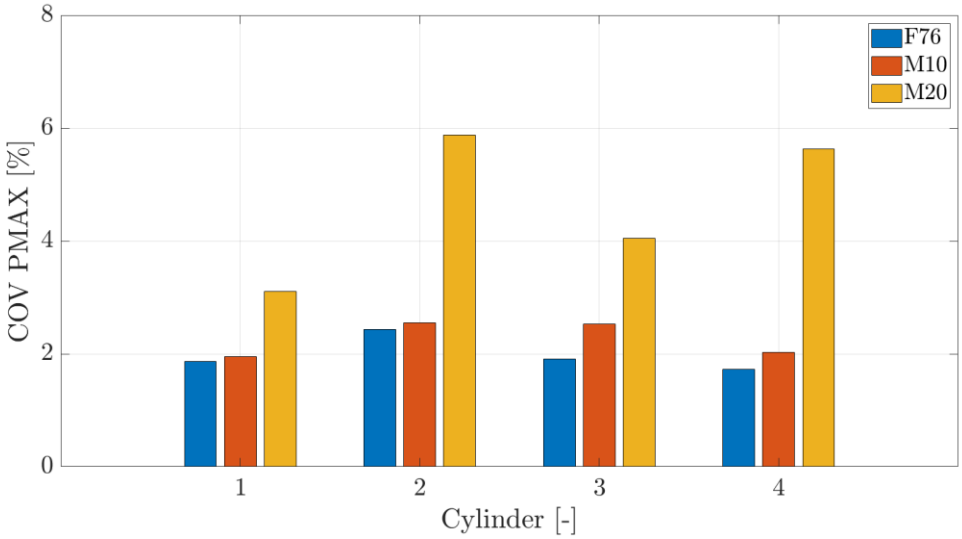

Figure 45: COV for maximum pressure of all cylinders, at measurement point 180 kW and 950 rpm

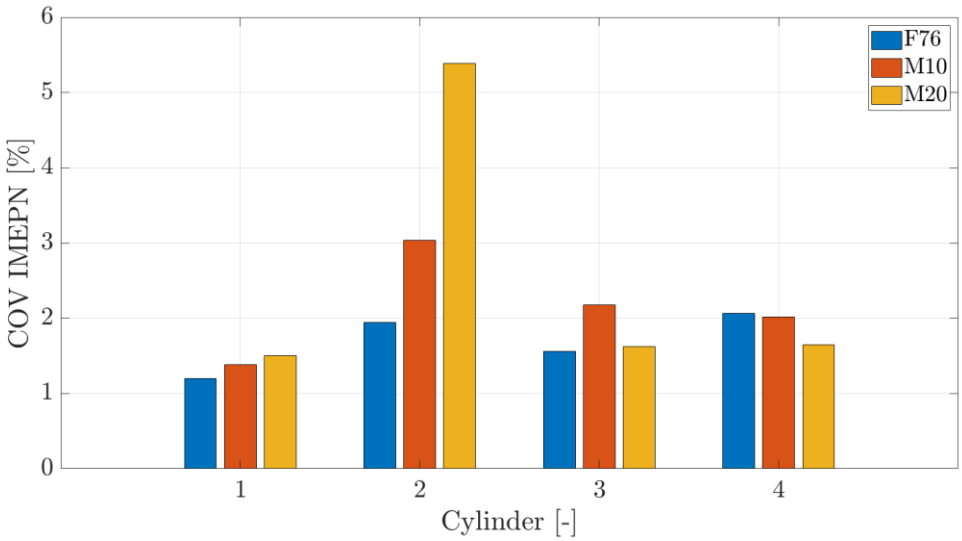

Figure 46: COV for IMEP of all cylinders, at measurement point 180 kW and 950 rpm

Running on M20 was only possible at higher engine load. At lower loads combustion did not take place in cylinders 2, 3 and 4. Only cylinder 1 could run at lower loads.

Figure 47 shows the mean pressure signal of cylinder 2, 3 and 4 for F76, M10 and M20 at 180 kW and 950 rpm. The curve of M20 reveals an ignition delay of 6° CA,

where the ignition delay of M10 is around 2° CA. Besides the late combustion, the curves show a steeper pressure increase after start of ignition, and comparable maximum pressures. Late combustion is equivalent for all mixtures.

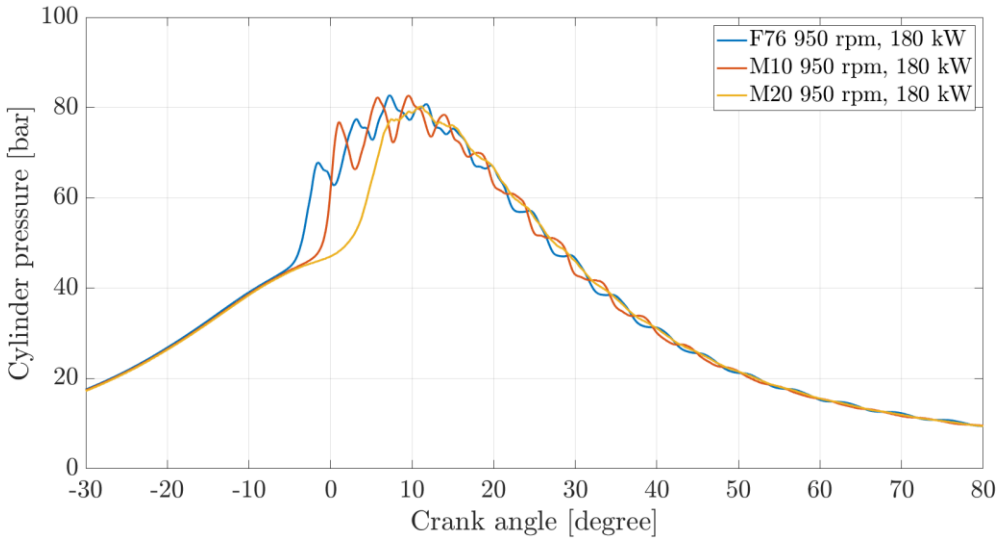

Figure 47: In-Cylinder mean pressure for F76, M10 and M20 of cylinder 2,3 and 4 at 950 rpm and 180 kW

6.3.5 *Combustion duration*

Tol used almos the same definition as Bosklopper to identify start of combustion and combustion duration, but he defined start of combustion at 5 % of the fuel combusted. Table 12 shows the data for measuring point 180 kW and 950 rpm/ The trends are comparable to the trands observed by Bosklopper. Start of ignition is delayed significantly, but difference decrease with increasing combustion rate. There is a strong decrease in combustion duration.

Table 12: Mean of kibox CA05, CA50 and CA90 values of the four measured cylinders (950 rpm; 180 kW)

	F76	M10	M20
CA05	-3.5	-0.9	4.4
CA50	23.0	18.9	14.9
CA90	76.5	75.4	72.7
CA90-C05	80	76.3	68.3

6.3.6 *Mean effective pressure*

Figure 48 shows the calculated mean effective pressure (IMEP) at the different measurement points of the grid. For M20 we could not perform measurements at low engine load as evaporation of the methanol required too much time to form an ignitable mixture in the cylinder. When comparing the values we found no significant difference in IMEP for the different mixtures.

The combustion problems are a major drawback for use of methanol when directly injecting in the cylinder. We can expect some benefits of injecting earlier during compression, which gives more time for methanol to evaporate, and injecting with

higher pressures, resulting in smaller droplet diameters which may speed up the evaporation process. However, the problems emerged already at M20, with only 35 % volumetric methanol content.

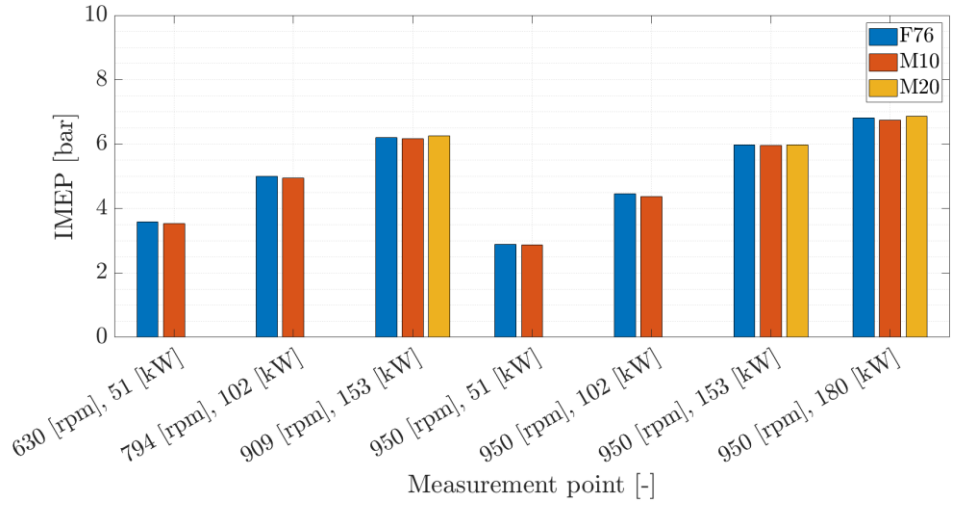

Figure 48: IMEP at the different measurement points

6.3.7 *Efficiency*

Figure 49 shows the engine efficiency at the different points of the measurement grid. The efficiency reported by Tol is the brake thermal efficiency: the measured brake power at the propeller shaft divided by the total amount of energy injected with the fuel. The figures shows no significant variation of the engine efficiency with increasing methanol content. The slightly later combustion will have a positive impact on the efficiency, but when ignition is delayed too much, efficiency will again decrease.

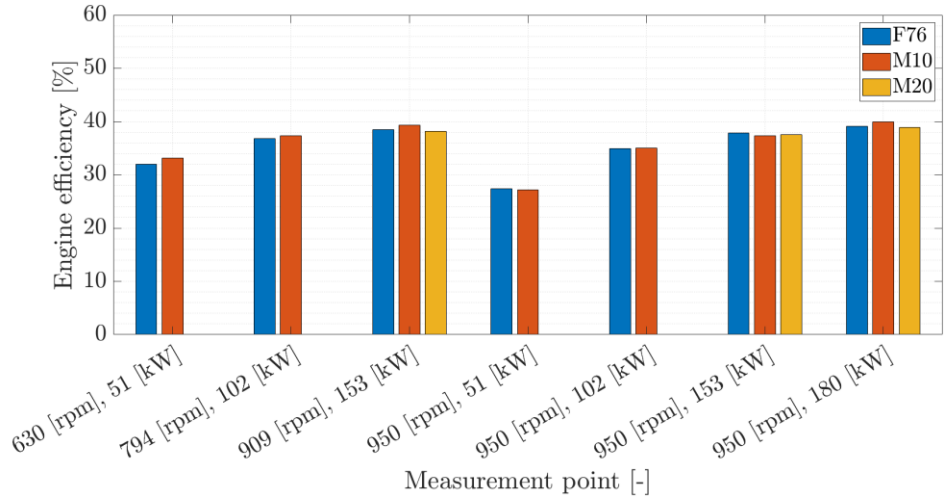

Figure 49: engine efficiency at the different measurement points

In itself this result is not too negative. We did not adapt injection timing (which is hardly possible for this engine with mechanical fuel injection). Modern engines –

where injection can be varied – offer the possibility of early fuel injection which help finding an optimum balance and optimize efficiency.

6.3.8 *Exhaust gas temperature*

We measured the exhaust gas temperature after the turbine and not directly after the cylinder. This results in lower temperatures compared to what we would expect directly after the cylinder. Nevertheless the observed differences in exhaust gas temperature give some indication about the combustion process.

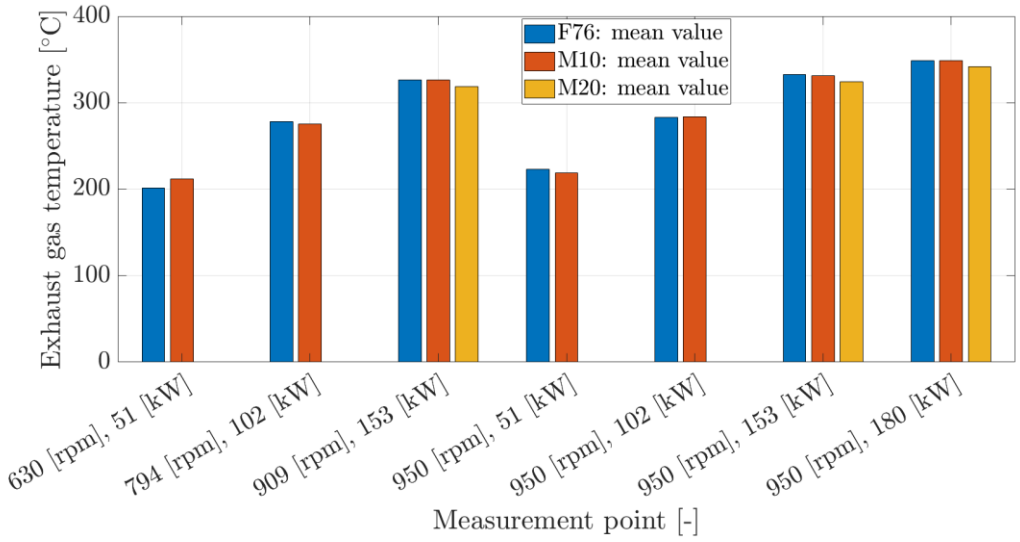

Figure 50: exhaust gas temperature (°C)

Figure 50 shows the measured exhaust gas temperature for the different points of the measurement grid. In almost all cases we found some decrease of the exhaust gas temperature for increasing methanol content. This is an indication of lower in-cylinder temperatures which relate to reduced NOx levels, but are also an indication of decreased in-cylinder temperatures.

Figure 51 shows the measured NOx emissions. Compared to F76, NOx emissions first decrease for M10, indicating lower peak temperatures in the cylinder. For larger Methanol content, NOx levels rise again for lower brake power. This is an indication that during combustion there are more and higher temperature hot spots. At higher break power NOx emissions reduce again with roughly 10 % compared to F76. We postulate this is the result of incomplete evaporation at earlier stages of combustion, resulting in spots with high methanol content resulting in hot spots during later stages. Earlier methanol injection combined with higher injection pressure could reduce NOx emissions for lower loads.

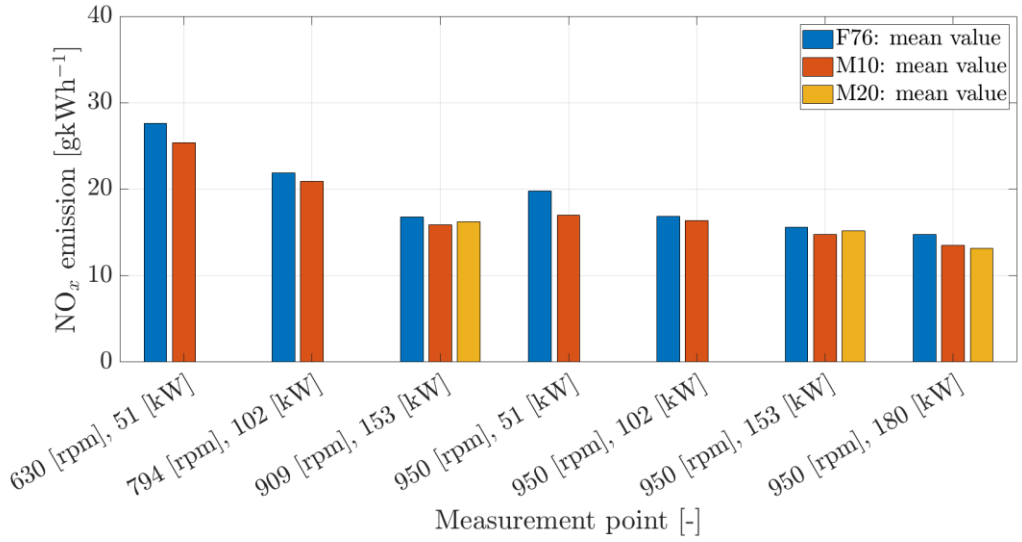

Figure 51: NOx emissions measured in the exhaust gas

Figure 52 shows the amount of unburned hydrocarbons measured in the exhaust gas. In all cases the amount of unburned hydrocarbons increased with methanol content. However, the measurement were not repeatable, indicating unstable combustion process. Another reason was found in the measurement set-up. Unburned hydrocarbons could – as side effect of the low temperatures in the exhaust hose – condensate against the hose wall, resulting in large measurement variations.

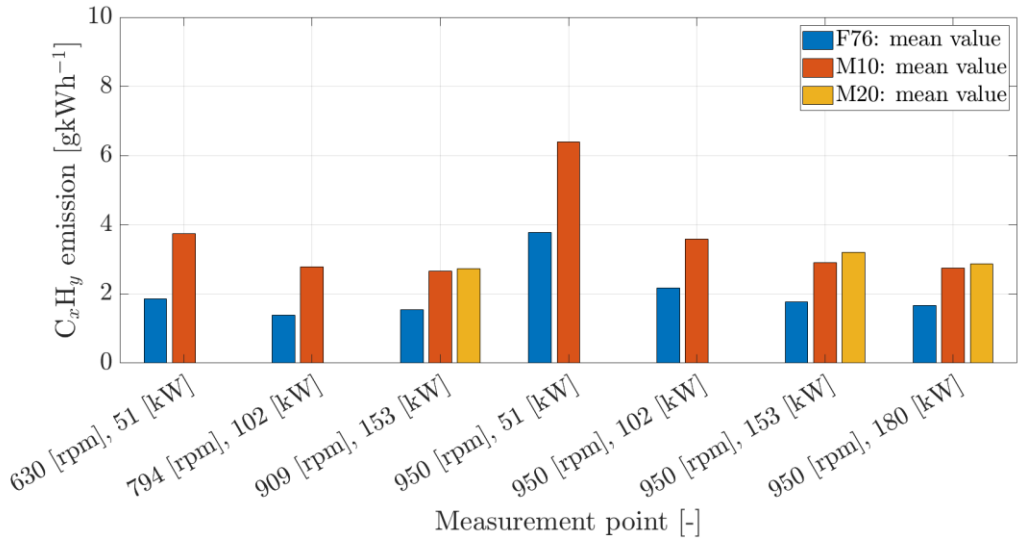

Figure 52: unburned hydro carbons measured in the exhaust gas

6.4 Modelling

6.4.1 *The in-cylinder model*

The in-cylinder model has been described in paragraph 5.4.1 and in Figure 26and Figure 27.

The model uses several assumptions and simplifications:

- The fuel injected directly evaporates and combusts. Injection rate equals combustion rate.
- The mass inside the cylinder is constant except the fuel injection rate. In reality fuel may leak resulting in a decrease of the total in-cylinder mass. This is however often neglected.
- The model assumes the ideal gas law is valid
- Fuel leakage between piston rings and cylinder wall is neglected
- Heat losses are only transferred to cylinder wall, cover and piston head.
- Atmospheric conditions are constant
- Ilnet receiver temperature is constant
- Cylinder wall, cover and piston head temperatures are constant

Tol adapted the Woschni parameters for the specific geometry of this engine. The Woschni parameters are identical for methanol and for diesel

Table 13: Woschni parameters used by Tol

parameter	Diesel	Methanol	Unit
C3	$2.28 + 0.308\frac{c_c}{c}m$	$2.28 + 0.308\frac{c_c}{c}m$	[-]
C4	$3.24 \cdot 10^{-3}$	$3.24 \cdot 10^{-3}$	$\left[\frac{m}{s \cdot K}\right]$
C1	127.93	127.93	[-]

6.4.2 *Methanol as fuel*

Lee [Lee 2016] added the chemical properties of methanol to the in-cylinder model for dual fuel operation. Lee assumed that methanol enters the engine in vapor phase using premixed port injection. Lee used diesel fuel as pilot fuel to ignite the premixed methanol-air mixture. For this study the model had to be further adapted to include vaporization of methanol in the cylinder.

Methanol has a much higher heat of vaporization than other fuels. As result, Tol had to adapt the model with respect to the first assumption.

6.4.3 *Injection model*

Tol used the plunger injection model of Zeng [Zeng 2019] to simulate the injection rate of the fuel. The plunger injection model is constructed by three separate models: a cam model, plunger pump model and an injector model. In his thesis Tol describes the equations governing the injection model.
The pump pressure is calculated using equation (9).

$$P_{pump} = \frac{K_f}{V_p}\left(\dot{Q}_{in} - \dot{Q}_{out} + \dot{V}\right) \quad (9)$$

Where
P_{pump} = pump pressure [N m^{-2}]
$\dot{Q}_{in}$ = volume flow into the pump chamber [m^3 s^{-1}]
$\dot{Q}_{out}$ = volume flow out of the pump chamber as result of spill leakage and flow to the injector [m^3 s^{-1}]
$\dot{V}$ = volume flow dictated by the movement of the cam [m^3 s^{-1}]
K_f = bulk modulus of the injected fluid [N m^{-2}]
V_p = Volume of the pump chamber [m^3]

The volume flow out of the injector is calculated by equation (10):

$$\dot{Q}_{out,cylinder} = C_{d,nozzle} \cdot A_{nozzle} \sqrt{\frac{2}{\rho_{liq}} \cdot \left|P_{nozzle} - P_{cyl}\right|} \quad (10)$$

Where
$\dot{Q}_{out,cylinder}$ = volume flow out of the injector into the cylinder [m^3 s^{-1}]
$C_{d,nozzle}$ = discharge coefficient of the nozzle [-] (see Figure 53)
A_{nozzle} = nozzle effective area [m^2]
ρ_{liq} = density of the injected fluid [kg m^{-3}]
P_{nozzle} = pressure in the nozzle [N m^{-2}]
P_{cyl} = pressure in the cylinder [N m^{-2}]

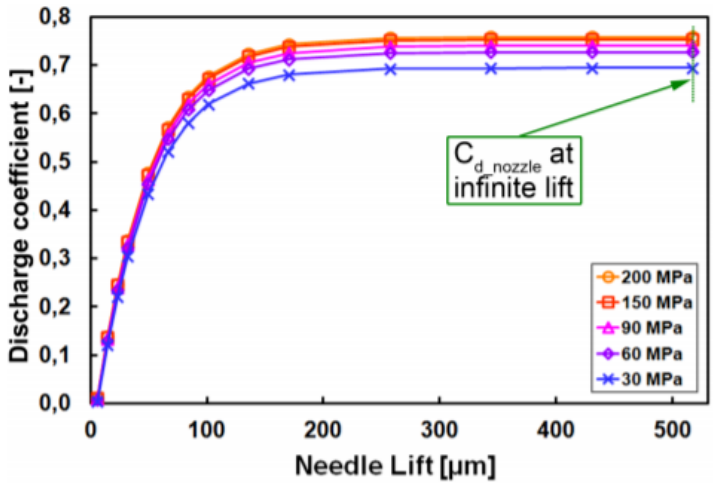

Figure 53: Relation between needle lift and discharge coefficient used by Tol

6.4.4 *Spray development*

Tol added a spray development submodel. After injection, the droplets in the fuel spray are gradually heated and evaporate to a stoichiometric gas mixture. Heat transfers from the surrounding cylinder to the droplets and mass is transferred from the droplet to the surrounding in-cylinder environment. Figure 54 show the different phases.

Directly after injection, the fuel breaks up into small droplets in liquid phase which is referred to as the spray formation and spray atomization. The small droplets start to heat up due to heat transfer from the gases in the cylinder. Pressure in the cylinder has an important impact on the heating period of the liquid droplets. Under constant pressure, the boiling temperature of liquids is constant. However, during the compression stroke the pressure rises and increases the boiling temperature of the substance which cause liquid to heat up to higher temperatures in order to vaporize during compression.

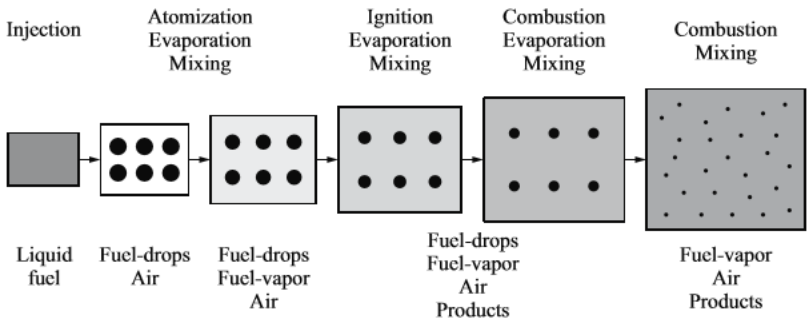

Figure 54: Spray development and evaporation after injection in the cylinder [Merker 2014]

Once the droplets starts to boil, drop evaporation causes mass transfer from fuel to air. During this process, vapor flows into the cylinders surrounded gases and form a combustible mixture. This process is usually referred to as air entrainment, the mixing of hot air with liquid and vapor fuel, important to get the fuel vaporized and creating an ignitable fuel mixture in the cylinder. Convective- and radiative heat transfer from the cylinder walls participate in the heating process. If the air-fuel mixture is lean, combustion might not get started. Rich fuel mixtures, high fuel/air ratios, could cause hot spots in the cylinder and local high ratios NO_x formation. Therefore, the quantity of fuel injected and the geometric properties of the injector are important for mixture formation.

During ignition, liquid droplets are still present in the cylinder in which a mixture of stoichiometric gas, fuel vapor and liquid exist. Heat from the flame front evaporates the remaining fuel before its ignition. At the end of combustion, often it is assumed that all fuel is burned and only stoichiometric gas and excess air are present in the cylinder. In real combustion processes, incomplete combustion decreases the energy released from the injected fuel and the engines efficiency. Chemical components such as CO, unburned hydrocarbons and soot in the exhaust gases are present and indicate whether combustion

was complete. Mainly incomplete combustion is caused by lack of oxygen [Merker 2014].

6.4.5 *Single droplet evaporation model*

The evapozation model is built on the work of Galindo [Galindo 2014]. Galindo developed a liquid zone model for diesel injection in a diesel engine. In this model

he described the liquid phase and its evaporation process after injection. Most complex phenomena during

spray development are not implemented in the model and replaced by assumptions to keep calculation times short. The model however is able to describe the heat and mass transfer processes in detail.

Adding a liquid zone to the dual fuel single zone model improves the description of the evaporation process. The development of the model starts by building a unsteady single droplet evaporation model for methanol and diesel droplets.

The main goal of this part of the work of Tol is to increase the accuracy of the model regarding the heat of vaporization of methanol. By building a single droplet evaporation model for methanol and diesel he could investigate the differences in the evaporation process of both fuels. After verifying the evaporation models, h calculated the heat of vaporization of the complete fuel spray are calculated. Tol did not adapt the evaporation heat loss model for diesel fuel.

The evaporation process in the cylinder is difficult to measure directly. The single droplet evaporation model gives an indication of the evaporation process of alcohol blends. The differences in evaporation speed and required heat calculated by the model are expected to be seen in the experiments from the pressure signal. For instance, the start of combustion is expected to be delayed.

6.4.6 Droplet formation

Droplet formation is important for the evaporation process: too large droplets needs too much time to evaporate and cause wall impingements. Droplet size is, except chemical properties, dependent on the nozzle diameter, injection pressure and cylinder pressure. A widely used method to describe the droplet size in a fuel spray is the sauter mean diameter (SMD).

The SMD approach approximates all the droplets to be equal in volume and diameter. The total volume of the fuel injection is the sum of all the droplets in the spray. The size of the droplets determines the evaporation efficiency and the time for the droplet to evaporate under given conditions. Moreover, the combustion is related to the mixture of air and fuel which is also dependent on the fuel drop size. Hiroyasu [Hiroyasu 1983] described the SMD for fuel sprays as given in equations (11), (12) and (13).

$$SMD_1 = 4.12\, d_0 \cdot Re_{liq}^{0.12} \cdot We_{liq}^{-0.75} \left(\frac{\mu_{liq}}{\mu_{gas}}\right)^{0.54} \cdot \left(\frac{\rho_{liq}}{\rho_{gas}}\right)^{0.18} \quad (11)$$

$$SMD_2 = 0.38\, d_0 \cdot Re_{liq}^{0.25} \cdot We_{liq}^{-0.32} \left(\frac{\mu_{liq}}{\mu_{gas}}\right)^{0.37} \cdot \left(\frac{\rho_{liq}}{\rho_{gas}}\right)^{-0.47} \quad (12)$$

$$SMD = \max[SMD_1, SMD_2] \quad (13)$$

With $We_{liq} = \frac{v_{liq}^2 \cdot d_o \cdot \rho_{liq}}{\sigma_{liq}}$: the Weber number of a droplet

And $Re_{liq} = \frac{v_{liq} \cdot d_0 \cdot \rho_{liq}}{\mu_{liq}}$: the Reynolds number of a droplet

Where:

SMD_x	= Sauter mean diameter	[m]
d_0	= diameter of the injection nozzle opening	[m]
v_{liq}	= liquid velocity	[m s^{-1}]
ρ_{liq}	= density of the fluid	[kg m^{-3}]
σ_{liq}	= surface tension	[N m^{-1}]
μ_{liq}	= dynamic viscosity of the fluid	[N s m^{-2}]
μ_{gas}	= dynamic viscosity of the gas	[N s m^{-2}]

When the *SMD* is known, the number of droplets can be calculated from the injected volume and droplet volume.

6.4.7 *Heating up the droplet*

Tol describes in his thesis how he models the heating process of the droplet. He only uses convection as way of heat transfer, ignoring radiation as a source. He did not take deformation, collisions and other interactions into account. The temperature in the cylinder is assumed constant in the entire cylinder. Turbulence in the cylinder is neglected even though this has an important impact on the mixing process of fuel and air. The droplets are assumed to be equally distributed within the spray, so each droplet undergoes the same process at the same time. The temperature in the droplet is assumed constant.

For heat balance, Tol based himself on the vaporization theory of Borman [Borman 1998], as described in equation (14.

$$m_{f,liq} \cdot c_{p,f,liq} \cdot \frac{dT_{f,liq}}{dt} = \widetilde{h*} \cdot A_0 \cdot \left(T_\infty - T_{liq}\right) - \dot{m}_{evap} \cdot h_{fg} \quad (14)$$

With:

$m_{f,liq}$ = mass of the fluid [kg]

$c_{p,f,liq}$ = heat capacity at constant pressure [kJ kg^{-1} K^{-1}]

$\widetilde{h*}$ = convective heat transfer coefficient determined by Nusselt number [$Wm^{-2}K^{-1}$]

A_0 = the area of the fuel droplet exposed to heat from the cylinder [m^2]

T_∞ = the cylinder temperature [K]

t = time [s]

T_{liq} = the droplet temperature [K]

$\dot{m}_{evap}$ = mass evaporated per second [kg s^{-1}]

h_{fg} = the difference between liquid and vapor enthalpy of the fuel [kJ kg^{-1}]

Tol corrected the heat transfer coefficient for high rates of vaporization. As explained in [Borman 1998] this leads to increased ambient temperatures near the droplet (equation (15) .

$$\widetilde{h*} = \tilde{h} \cdot Z = \tilde{h} \cdot \frac{z}{e^z - 1} \tag{15}$$

With:

$$z = \frac{\dot{m}_{evap}}{\tilde{h} \cdot A_0} \tag{16}$$

Although the difference between liquid and vapor enthalpy of the fuel is dependent on temperature, Tol kept this term constant during the vaporization process. This leads to an underestimation of the vaporization rate at later stages of the compression process and during the early stages of combustion, against an overestimation in the early stages, just after injection.

6.4.8 Mass transfer

The difference between the vapor pressure and the cylinder pressure is the driving force for vapor the move away from the droplet. Tol calculated the mass transfer rate using the Sherwood number Sh to calculate the mass transfer film coefficient $\tilde{h}_d$ (eq (17).

$$Sh = \frac{\tilde{h}_d \cdot d}{D_{AB}} = 2 + 0.6 \cdot Re^{1/2} \cdot Sc^{1/3} \tag{17}$$

In this equation, Sh is the Schmidt number.

Further:

μ = the dynamic fluid viscosity [N s m^{-2}]

ρ_f = the fluid density [kg m^{-3}]

$\tilde{h}_d$ = mass transfer film coefficient [m s-1]

d = the droplet diameter [m]

D_{AB} = the mass diffusivity coefficient [cm^2 s^{-1}]

Tol used the following equations for Methanol in air (D_{MA}) and diesel in air (D_{DA}):

$$D_{MA} = e^{(4.4426 \ln(T) - 27.056)} \tag{18}$$

$$D_{DA} = (-0.02513 + 0.00013439T + 3.1511 \cdot 10^{-7} \cdot T^2) \cdot 10^{-4} \tag{19}$$

Where T is the mean of the film temperature and the environmental temperature of the droplet.

This mass transfer coefficient is correct for low vaporization rates. Tol used the correction factor decribed by Borman [Borman 1998] to correct for high vaporization rates:

$$\frac{\tilde{h}_d^*}{\tilde{h}_d} = \ln\left(\frac{p - p_{v,\infty}}{p - p_{v,0}}\right) \cdot \frac{p}{p_{v,0} - p_{v,\infty}} \tag{20}$$

Where

p = the cylinder pressure [N m^{-2}]

$p_{v,\infty}$ = the vapor pressure in ambient conditions [N m^{-2}]

$p_{v,0}$ = the saturated vapor pressure at droplet temperature and cylinder pressure

Now the vaporization rate can be written as:

$$\dot{m}_{evap} = \tilde{h}_d^* \cdot A_0 \cdot \left(p_{v,0} - p_{v,\infty}\right) \tag{21}$$

And after substitution:

$$\dot{m}_{evap} = Sh \cdot \pi \cdot d \cdot \rho_f \cdot \ln\left(\frac{p}{p - p_{v,0}}\right) \tag{22}$$

6.5 Model Analysis

A four-stroke diesel cycle contains a compression, expansion, outlet and inlet stroke. For study of heat release measurements, the in- and outlet stroke are thermodynamic less of interest, as these models aim to study and optimize the thermodynamic process during compression and expansion. Therefore, the models used by Tol [Tol 2020] only calculate the process from inlet valve closes (IC) until exhaust valve opens (EO).

6.5.1 Heat release

Stapersma [Stapersma 2003] argues that heat release can be studied using a single zone model that uses pressure signals correlated to in-cylinder pressure. The combustion inside the cylinder takes place in a single volume with no distinct difference between the unburned fuel and air zone. This is a simplification from reality where multiple zones of with air-fuel mixtures varying from completely unburned fuel up to hot areas where all fuel is combusted. As result the output of a single zone approach is evaluated as a mean value of the complete cylinder volume.

6.5.2 Injection model

Results from the injection model are used in the calculation of the fuel spray heat of evaporation. The injected volume flow into the cylinder and droplet diameter are the most important results calculated by this model.

The adapted injection model contains one unknown: the nozzle discharge coefficient. When the model correctly models all processes in the entire injection

system, a single tuning parameter should be sufficient for all conditions. As Table 14 shows, the discharge coefficient is not constant, so we have to further tune the injection model.

Table 14: Injection model discharge coefficient

Fuel	Speed (rpm)	Load (kW)	Discharge coefficient (-)
F76	909	153	0.85
F76	950	153	0.86
F76	950	180	0.91
M10	909	153	0.95
M10	950	153	0.99
M10	950	180	1
M20	909	153	0.94
M20	950	153	0.94
M20	950	189	0.98

To accommodate for this issue, we created a correlation between fuel rack and engine power for the three different fuels, as shown by equations (23(24(25)

$$RACK_{F76} = 5.95 \cdot 10^{-2} \cdot P_{brake} + 5.28 \quad (23)$$

$$RACK_{M10} = 5.25 \cdot 10^{-2} \cdot P_{brake} + 6.28 \quad (24)$$

$$RACK_{M20} = 7.69 \cdot 10^{-2} \cdot P_{brake} + 4.07 \quad (25)$$

Where:

$RACK_{xab}$ = fuel rack position of fuel xab [mm]

P_{brake} = brake power [kW]

6.5.3 *Vaporization model*

Tol first validated his model by literature data, using a study on the evaporation of decane droplets of 2 mm in air with atmospheric pressure at a temperature of 1000 K. The study revealed an initial period with constant droplet diameter, where the droplet was heating up, followed by a linear decrease of the droplet in time.

With use of a dimensional analysis we found a relation between the time required for heating up the droplet dependent on droplet diameter. We found that the thermal gradients within the droplet can be ignored as result of the very small droplet size of around 10 μm.

Wang [Wang 2017] studied the evaporation rate of methanol droplets of different diameters using a high speed camera and temperatures. We validated our model against the results of Wang, assuming zero speed of the droplets in the model of Wang.

In this way, we obtained a model we could use to calculate the evaporation rate, calibrated for 0 speed. Using the evaporation enthalpy we could determine the required heat in time to evaporate the droplets of methanol and diesel in time. In this model we assumed a constant pressure of 700 K and a pressure of 1 bar. This

was done to limit computation time. In the future, the evaporation model needs to be extended to correct for changing temperatures and in cylinder pressure during the evaporation process. Figure 55 shows the resulting required evaporation heat for M20, for various droplet sizes.

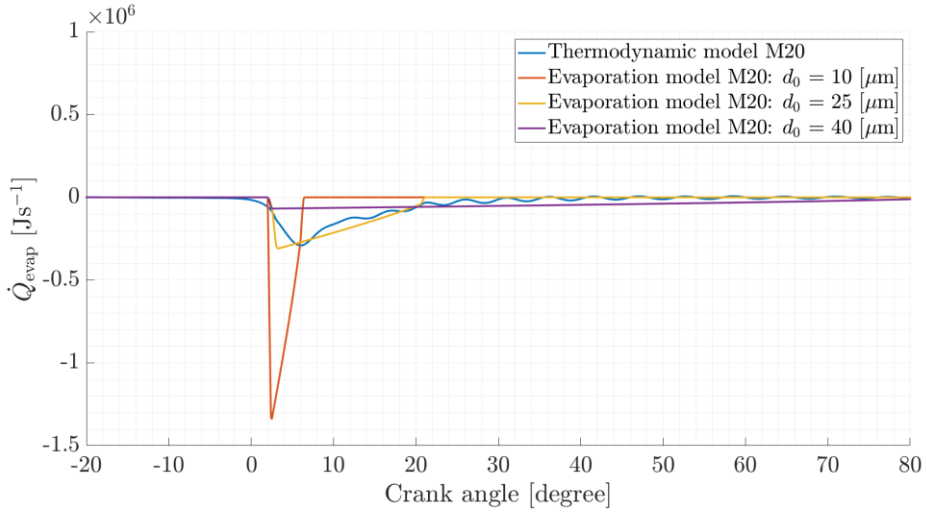

Figure 55: Evaporation heat vs crank angle

The figure clearly shows the increased required time to evaporate increasing droplet diameters. Tol compared the results of the evaporation model with calculated heat release from the engine. He concluded that the results of a droplet diameter of 25 µm best represented reality. Figure 55 also clearly shows that evaporation time decreases with decreasing droplet diameter. A smaller droplet diameter gives us a completely evaporated mixture in earlier phases. Equations (11) and (12) indicate droplet diameter decreases with increasing speed, and increasing speed can be obtained by increasing pressure diameter, or decreasing diameter of the injection needle.

6.5.4 *Heat release*

Figure 56 shows the GAHRR at grid point 950 rpm and 180 kW. Heat release clearly delays with increasing methanol content. For F76 and M10 premixed combustion takes place before TDC, where M20 only shows premixed combustion after TDC. This delay is the result of the higher evaporation heat and bad ignition properties of methanol. After ignition, the mixture releases more heat during premixed combustion. As result, temperature increases more for M20 than for the other mixtures. Diffusive combustion phase almost disappeared and is visible only between 9° ATDC and 12° ATDC.

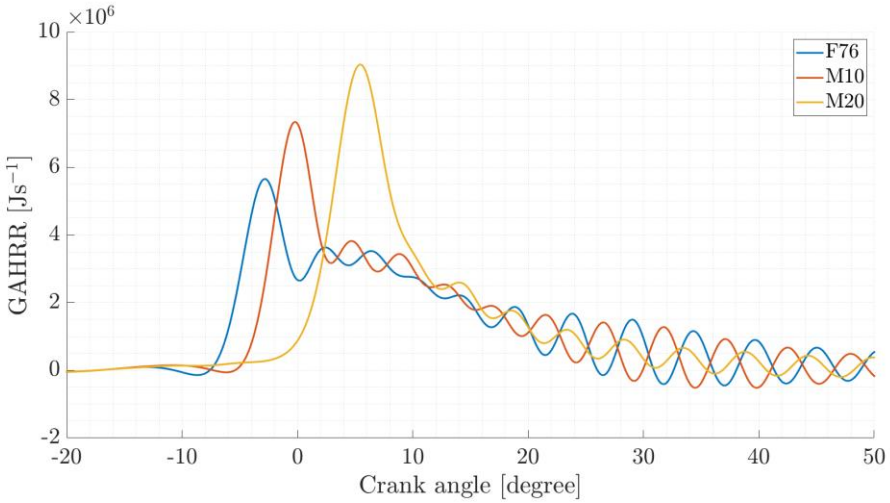

Figure 56: GAHRR vs crank angle at 950 rpm and 180 kW; cylinders two, three and four

In general methanol blends show larger premixed heat release rates compared to F76, at the cost of heat release during diffusive combustion and late combustion phases. From literature [Jamrozik 2017] we found this phenomenon lasts up to 25 % methanol, after which premixed combustion heat release rate decreases again. It is unclear in how far this finding holds for our experimental setup.

The heat release rate has influence on the engine's efficiency. For efficient engine operation, the ignition should take place close to TDC to exert maximum work during the expansion stroke. As result of the a large ignition delay of the M20 mixture, the piston already moved downwards without being pushed by the in-cylinder pressure. The crank angles without combustion aTDC are considered as an efficiency loss. This is an indication that for larger methanol content, early injection and smaller droplet size (higher injection pressure and smaller needle diameter) could help further improving efficiency.

6.5.5 *Temperature*

With use of the single zone model we calculated the temperature vs crank angle for all mixtures and all grid points (see Figure 57). As we use a single zone model, the figures do not provide information about local hot spots and cold spots in the cylinder during combustion. The calculated maximum temperature increases with methanol content, presumably resulting from the shorter and more intense premixed combustion phase. The period with highly elevated temperature (> 1200 K) decreases with increased methanol content. This could help improving the overall efficiency of the combustion process.

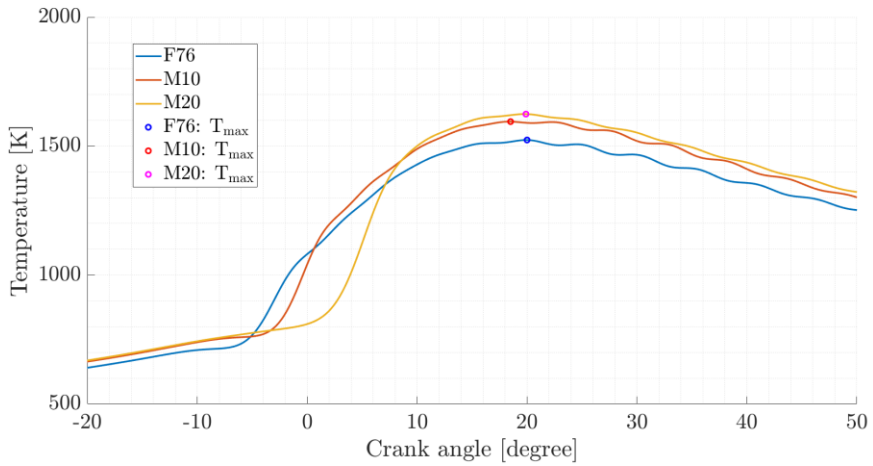

Figure 57: Calculated in cylinder temperature of F76, M10 and M20 for grid point 950 rpm and 180 kW

Based on these elevated temperatures we would expect clearly increased NOx emissions with increased methanol content. However, Figure 51 reveals slightly decreasing NOx emissions with increasing methanol content. We assume two possible reasons for this counter intuitive correlations. The duration at highly elevated temperatures is shorter, so there is less time for NOx formation. The second reason could be that the injection and combustion process enhance mixing before combustion, resulting in a more uniform temperature subdivision inside the cylinder and less distinguished hotspots. Multiple zone modeling is required to answer this question.

6.5.6 *Engine speed*

When comparing the calculated in cylinder temperature we found for all fuels an increase of the temperature with decreasing engine speed (Figure 58). We assume the reduced engine speed leaves more time for the fuel to evaporate before ignition starts, resulting in increased premixed combustion and faster ignition process.

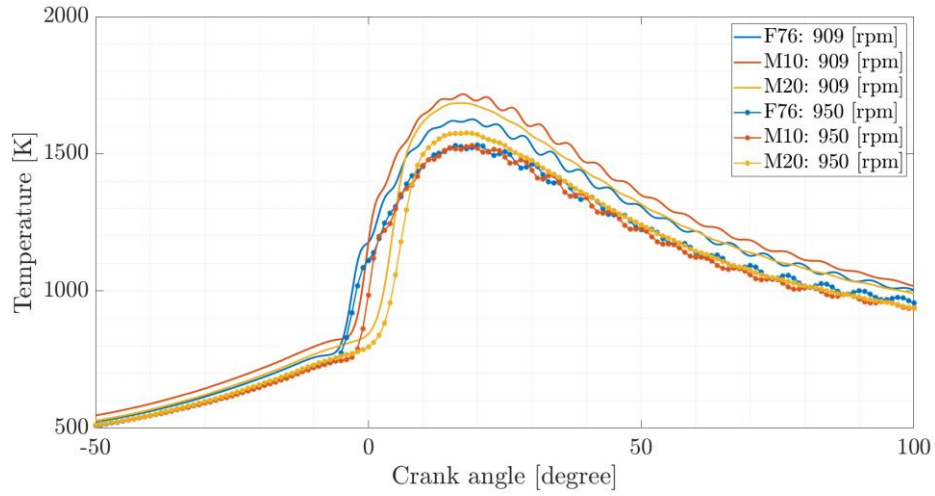

Figure 58: Calculated in cylinder temperature of F76, M10 and M20 for grid point 909 rpm and 950 rpm at 153 kW

This assumption is confirmed by a decreased ignition delay for M10 and M20 with decreased engine speed, the calculated RCO and the elevated NOx emissions at decreased engine speed which all indicate shorter premixed combustion and higher temperatures at decreased engine speed.

6.6 Conclusions

- Methanol has the disadvantage being toxic to primates. With additional air ventilation systems and personal protective gear as overalls, gloves and full face gas masks we could relatively easy adapt to obtain safe working conditions.
- The lower heating value of methanol, resulting in higher fuel flows at equal power, the four times higher heat of evaporation and the cetane number of 4 make compression ignition of methanol very challenging.
- During experiments, the engine is not able to maintain its operation envelope from a methanol ratio of 20 [% energetic]. At low loads, the engines temperature seems to be too low in order to vaporize the methanol in the engine. For M20, operation below 153 [kW] resulted in an engine failure due to failed ignition in the cylinders.
- We observed an elongated ignition delay up to 8°CA for M20. Combustion duration seems to decrease significantly with 12.7°CA, while the engine efficiency remained almost constant for M20.
- Combustion process stability decreased with increasing methanol content.
- NO_x emissions decreased with 2.9 up to 14.2 [%] by using methanol compared to F76. We assume the short combustion time and the cooling effect caused by evaporation of methanol are responsible for this difference.
- In cylinder temperatures and NO_x emissions increase with decrease in engine speed. We assume this is caused by better evaporation of the fuel before ignition leading to elevated premixed combustion and consequential elevated temperatures.
- The evaporation model gives us a reasonable approximation of the heat release rate before combustion.
- We found a significant increased evaporation time for methanol compared to F76. For low engine load this resulted in failure to ignite. For direct injection in the cylinder this phenomenon can be countered by decreasing droplet size (decreased opening of the injection needle and increased injection pressure) and by earlier injection of methanol.
- We found indications that efficiency can be improved when using methanol, compared to F76.

7 Conclusions

We can conclude the following:

- With an emulsifier we can obtain a stable F76–methanol solution for longer duration. The tests show that a stable emulsion appears when Hypermer B246-SO-(MV) (0.3 w/v%) is used. This mixture remained stable for more than 10 hours
- This emulsifier is the only one that could accomplish this result. Because of the small amount of emulsifier Hypermer B246-SO-(MV) pointed out to be quite effective.
- Our tests with Span 65 and Tween 80 (0,3 w/v%), in ratio 74,4:25,6 w% indicate that a small droplet size can be obtained, but the resulting mixture did not remain stable for a longer period than 4 hours.
- During the mixing process a significant part of the methanol evaporates (unless mixing takes place in a closed environment) for mixing durations over 45 minutes.
- We were able to refurbish both the spark ignited port fuel injection engine and a compression ignited direct fuel injection engine to run (partly on methanol) .
- Methanol has the disadvantage being toxic to primates. With additional air ventilation systems and personal protective gear as overalls, gloves and full face gas masks we could relatively easy adapt to obtain safe working conditions.
- The spark ignited engine can run stable on 100% methanol between 16 ^{0}CA BTDC and 24 ^{0}CA BTDC ignition timing.
- Our compression ignited direct injection engine could only run stable on a mixture up to 20 % energetic (37,5 % volumetric) of methanol over the main part of the original operating envelope of the engine.
- The stability of the in cylinder process of Methanol or Methanol-F76 mixtures is lower compared to natural gas and F76.
- We hypothesize stability could be improved by redesigning the engine to allow better evaporation of methanol before combustion, and by improving the injectors (higher injection pressures; smaller opening)
- In the spark ignited engine methanol shows 7.0 °CA's earlier CA50 and 2.6 °CA's earlier CA10 compared to NG. Indicating faster (premixed) combustion. But due to late CA90, the combustion duration is almost equal
- The compression ignited engine showed delayed combustion as result of the higher evaporation heat of methanol and the consequential too lean mixture in early stages. The premixed combustion phase in this engine was shorter for methanol mixtures compared to pure F76.
- A changing temperature after the cooler did not lead to significant changes calculated in the CA10, CA50, CA90 and the combustion duration although

we found more methanol being evaporated before entering the engine at elevated air temperatures after the cooler.

- Methanol shows steeper increase of pressure after TDC compared to NG and compared to pure F76, indicating faster combustion after TDC.
- In the spark ignited engine the maximum pressure increased and the position shifted closer to TDC, as ignition timing was advanced from 16 to 24 °CA BTDC, leading to engine efficiency improvements
- In the compression ignited engine maximum pressure also increased, but the position shifted more and more after TDC as methanol content increased.
- Maximum in-cylinder temperatures around 1400 K were reached for NG and methanol, as expected due to fixed NOx emission settings. With methanol maximum temperature was reached about 20 CA earlier.
- In the compression ignited engine NO_x emissions decreased with 2.9 up to 14.2 [%] by using methanol compared to F76, notwithstanding elevated maximum pressure with increased methanol content. We assume the short combustion time, the cooling effect caused by evaporation of methanol and better pre-combustion mixing are responsible for this difference.
- Maximum temperatures at an earlier CA results in a lower (in-cylinder) exhaust temperature. Methanol also has lower exhaust temperatures compared to NG, and with the ignition variation at an advanced ignition timing of 24 °CA BTDC.
- In the spark ignited engine efficiency improved by 0.9% and 2.2% with methanol compared to natural gas at same test conditions of power output, ignition timing and NOx emissions. These preliminary methanol engine results show that improvements in engine efficiency could be obtained from a retrofitted SI NG engine converted to operate on 100% methanol without making any modifications to the geometrical engine specifications such as cylinder or piston geometry.
- The maximum pressure increased and shifted closer to TDC with advanced ignition timing when operating on 100% methanol. Thus, leading to engine efficiency improvements of about 1.5% at advanced ignition timing of 24 ^{0}CA BTDC compared to 18 ^{0}CA BTDC.
- A decrease of 21 °C in maximum in-cylinder temperatures calculated at an increase of manifold temperature from 40 to 60 °C, at equal power output and equal fuel consumption. Lower in-cylinder temperatures are expected to relate to lower measured NOx emissions.
- Also for the compression ignited engine we found indication that efficiency can be improved when injection methanol-F76 mixtures compared to pure F76 injection.
- We assume that increasing the manifold temperature further improves in-cylinder performance until 100% vapor is reached at the moment of IVC.

8 Future research

Our attempts to keep a methanol-F76 mixture stable over longer periods using emulsifier showed a mixed success rate. We could keep the mixture stable in an enclosed day tank for longer periods by continuously stirring the mixture. But, extrapolating this results to a full scale situation on board of a ship does not give us high hopes. The day-to-day practice on a ship is less controlled than a lab situation. It is easy to make mistakes and this could lead to a completely separated diesel-methanol mixture in the day-tank. As results, sooner or later pure methanol will be injected in the engine, which doubtlessly leads to engine failure.

For the moment we renounce further research into stabilizing methanol-diesel mixtures. We consider it unlikely that on a commercial ship this mixing practice will be employed an a safe way. We believe our research should focus on injecting methanol and a pilot fuel separately in an internal combustion engine.

The experiments with the spark ignited engines were very hopeful. We could run on 100 % methanol and efficiency even improved slightly with indications of decreased NOx emissions. Our future research with the SI engine will focus on the following:

- Impact of increased air temperatures on the evaporation of methanol before entering the cylinder
- Impact of evaporated methanol percentage on the combustion process
- Impact of ignition timing on the combustion process
- Maximizing engine performance
- Pilot projects

The experiments with the direct injected compression ignited engines did not give very hopeful results.

- It is quite an issue to keep methanol and diesel mixed in a tank. In our lab setup we could keep both fluids well mixed by permanently mixing, but this is not a solution on board a ship.
- Our attempts to keep both fluids mixed with an inhibitor were not very successful.
- Translating our problems to full scale situations on board a ship reveals safety issues that are probably unacceptable from a safety point of view. Segregation of both fuels in a day tank will lead to injection of pure methanol sooner or later. This will lead to failure of the engine to ignite and black-out.

We think it may be possible to ignite a mixture with methanol and a pilot fuel in a compression ignited engine, but not in the way we tested in our lab. We see the following options

- Using a longer alcohol (pentanol, octanol) as pilot fuel. The chemical composition of these longer alcohol chains make it more likely methanol dissolves and remains dissolved in this alcohol.
- Longer alcohol chains have high cetane numbers, improving combustion characteristics
- Separate injection of methanol and a pilot fuel is another option, that may also work in smaller compression ignited engines.
    - Methanol could in these experiments be ignited directly but separate from the pilot fuel using two injection needles
    - This would require earlier injection of methanol at higher pressures enabling better pre combustion evaporation
    - Methanol can also be injected via the air. This enables methanol to evaporate to a large extent before entering the cylinder, giving us basically the same situation as with the spark ignited engine but now with a pilot fuel instead of a spark

9 References

[Agarwal 2019] A.K. Agarwal, N. Sharma, A.P. Singh, V. Kumar, D.P. Satsangi, and C. Patel, "Adaptation of methanol-dodecanol-diesel blend in diesel genset engine", *Journal of Energy Resources Technology, Transactions of the ASME*, 141(10): 1–9, 2019. ISSN 15288994. doi: 10.1115/1.4043390.

[Ali 1993] I. Ali and M. A. Basit, "Significance of hydrogen content in fuel combustion", *International Journal of Hydrogen Energy*, 18(12):1009–1011, 1993. ISSN 03603199. doi: 10.1016/0360-3199(93) 90083-M.

[Ayouril 2011] "Electro-steric stabilization", Available: https://commons.wikimedia.org/wiki/File:Electro-Steric Stabilization.jpg visited 23-11-2020.

[Borman 1998] G.L. Borman and K.W. Ragland, "Combustion Engineering", McGraw-Hill, 1998. ISBN 0-07-006567-5.

[Bosklopper 2020a] J. Bosklopper, "Experimenting and modelling heat release study on a 100% methanol port fuel injected spark ignited engine", MSc thesis, Delft University of Technology, Delft, august 2020.

[Bosklopper 2020b] J. Bosklopper, H.Sapra, R. van de Ketterij, W. van Sluijs, C. Bekdemir, P. de Vos and K. Visser "Experimental study on a retrofitted marine size spark-ignition engine running on port-injected 100 % methanol", INEC conference, Delft, October 2020.

[Ding 2011] Y. Ding, "Characterising Combustion in Diesel Engines: Using parameterised finite stage cylinder process models", Delft University of Technology, Delft, 2011. ISBN 9789065622891. URL https://repository.tudelft.nl/islandora/object/uuid{%}3A10e25404-4b8e-443b-9f16-5e6e5c2a7444?collection=research.

[Doetjes 2020] G.Doetjes, "Het bepalen van een geschikte emulgator om F76 en methanol gemend te houden", BSc Thesis, Nederlandse Defensie Academie, Den Helder, 17 april 2020.

[Eversdijk 2020] J.Eversdijk and F.F. Vercauteren, "Emulsification of methanol in diesel", Internal TNO report, 9 march 2020.

[Galindo 2014] S.G. López. "Three-Zone in-cylinder process model for DI diesel engines", 2014. doi: SDPO.14.010.m.

[Huang 2004] Z. H. Huang, H. B. Lu, D. M. Jiang, K. Zeng, B. Liu, J. Q. Zhang, and X. B. Wang, "Engine performance and emissions of a compression ignition engine operating on the diesel-methanol blends", *Proceedings of the Institution of Mechanical Engineers, Part D: Journal of Automobile Engineering*, 218(4):435–447, 2004. ISSN 09544070. doi: 10.1243/095440704773599944.

[Heywood 2015] J. B. Heywood, “Internal Combustion Engine Fundamentals”, vol. 21. 2015

[Hiroyasu 1983] H. Hiroyasu, “Development and use of a spray combustion modelling to predict diesel engine efficiency and pollutant emissions”, *Bulletin of the JSME*, 26:569–575, 1983.

[Jamrozik 0217] A. Jamrozik, “The effect of the alcohol content in the fuel mixture on the performance and emissions of a direct injection diesel engine fueled with diesel-methanol and diesel-ethanol blends”, Energy Conversion and Management, 148:461–476, 2017. ISSN 01968904. doi: 10.1016/j.enconman.2017.06.030. URL http://dx.doi.org/10.1016/j.enconman.2017.06.030.

[Jiao 2016] W. Jiao, Y. Wang, X. Li, C. Xu, Y. Liu, and Q. Zhang, “Stabilization performance of methanol-diesel emulsified fuel prepared using an impinging stream-rotating packed bed,” Renewable Energy, vol. 85, pp. 573–579, 2016

[Ketterij 2018] R.G. van de Ketterij, “Emissions reduction at the Netherlands Ministry of Defence: potential, possibilities and impact”, INEC Conference, Glasgow, UK, October 2 – 4, 2018. Doi 10.24868/issn.2515-818X.2018.065.

[Kistler 2017] “Kibox type 2893 specifications sheet”, Technical report, 2017. URL: https://www.kistler.com/en/product/type-2893b/ visited 27-10-2020

[Kistler 2009] Kistler, “Pressure sensor 7061B specifications sheet”, Technical report, 2009.

[Lee 2016] B. Lee, “The effects of methanol fuel on combustion in premixed dual fuel engine” Delft University of Technology, Delft, 2016.

[Merker 2014] G. Merker, C. Schwarz, G.R. Stiesch and F. Otto, “Simulating Combustion: Simulation of combustion and pollutant formation for engine-development”, Number 1. 2014. ISBN9780874216561. doi: 10.1007/s13398-014-0173-7.2.

[Methanol Institute 2008] Methanol Institute, “Methanol Safe handling manual”, Technical Report dated October 2008.

[Pon Power 1993] PON Power, “Caterpillar gas engine data ID: APERFAB30”, vol. 1. August, 1993.

[Sapra 2019] H. Sapra, Y. Linden, W. van Sluijs, M. Godjevac, and K. Visser. “Experimental investigations of performance variations in marine hydrogen-natural gas engines”, *Cimac Congress 2019*, 2019, pp. 1–17.

[Sapra 2020] H. Sapra, M. Godjevac, P. d. Vos, W.v. Sluijs, Y. Linden, and K. Visser, “Hydrogen-natural gas combustion in a marine lean-burn SI engine: A comparitive analysis of Seiliger and double Wiebe function-based zero–dimensional modelling” Energy Conversion and Management,207(January):112494,2020.ISSN01968904. doi: 10.1016 /j.enconman.2020. 112494. URL https://doi.org/10.1016/j.enconman.2020.112494.

[Sapra 2020b] H. Sapra, J. Stam, J. Reurings, L. Van Biert, W. Van Sluijs, P. de Vos, K. Visser, P.V. Aravind, and H. Hopman. “SOFC-ICE Integration for maritime applications”, *To be Published*, pages 1–50, 2020

[Stapersma, 2003] D. Stapersma, “Diesel Engines Volume 3, Combustion”, Den Helder 2003. ISBN 0693485000.

[Stapersma 2010] D. Stapersma, “Diesel Engines Volume 1 Performance Analysis”, Lecture notes WB4408A, 1, January 2010

[Stapersma 2010b] D. Stapersma, “Diesel Engines Volume 4 Emissions and Heat transfer” April 2010, volume 4. 2010. ISBN 0693485000

[Stapersma 2010c] D. Stapersma, “Diesel Engines Volume 5 Thermodynamical Principles I”, 2010. ISBN0693485000.

[Stapersma 2010d] D. Stapersma, “Diesel Engines Volume 3 Combustion” April 2010, ISBN 0693485000.

[Stapersma 2010e] D. Stapersma, “Diesel Engines Volume 6 Thermodynamical Principles II”, 2010.

[Tadros 2016] T. F. Tadros, “Emulsions: Formation, stability, industrial applications”, Walter de Gruyter GmbH & Co KG, 2016.

[Tol 2020] R.Tol “Combustion of diesel-methanol blends in a compression ignited engine”, MSc Thesis, Delft University of Technology, Delft, august 2020.

[Verhelst 2019] S. Verhelst, J.W.G. Turner, L. Sileghem and J. Vancoillie, “Methanol as a fuel for internal combustion engines”, Progress in Energy and Combustion Science, 70:43–88, 2019. ISSN 03601285. doi: 10.1016/j.pecs.2018.10.001.

[Wang 2017] F. Wang, J. Yao, S. Yang, R. Liu, and J. Jin, “A new stationary droplet evaporation model and its validation”, Chinese Journal of Aeronautics, 30(4):1407–1416, 2017. ISSN 10009361. doi: 10.1016/j.cja.2017.06.012. URL http://dx.doi.org/10.1016/j.cja.2017.06.012.

[Xie 2013] F. Xie, X. Li, X. Wang, Y. Su, and W. Hong, “Research on using EGR and ignition timing to control load of a spark-ignition engine fueled with methanol”, Appl. Therm. Eng., vol. 50, no. 1, pp. 1084–1091, 2013

[Zeng 2019] J. Zeng, “Modelling and simulation of the Diesel Engine Injection Systems”, TU Delft Master Thesis, 2019. ISSN 1098-6596. doi: 10.1017/CBO9781107415324.004

A.1 Description of the Measurement equipment

A.1.1 Testo-350 (Maritime) gas analyser

The testo-350 was used in both experimental setups to measure the emissions (except for the unburned hydrocarbons. Figure 59 shows the Testo-350. Table 15 gives the specifications of the testo-350 gas analyser.

Figure 59: the teso 350

Table 15: Specifications of the testo 350 gas analyser

Parameter	Range	Unit	Tolerance
NO_x	0 to 3000	[ppmv]	±5 [%] (NOx)
SO_x	100 to 3000	[ppmv]	±5[%]
CO_x(IR)	0 to 40	[vol.%]	±0.5 [vol.%]
CO	0 to 3000	[ppmv]	±5 [%]
O_2	0 to 25	[vol%]	±0.2 [vol.%]
°C, flue gas	-40 to +1000	[°C]	±5 [°C]
C_xH_y	100 to 4000	[ppmv]	±400 [ppmv]

A.1.2 *Kibox 2893A*

The Kibox 2893 is used in both experimental setups. The technical data specifications are specified in [Kistler 2017]. Table 16 gives the specifications of the Kibox sensors used in the spark ignited tests.

Table 16: Specifications of the Kibox sensors used for the Spark Ignited tests

Kibox sensors	use	range	accuracy
In cylinder pressure sensor	In-cylinder pressure (cylinder3,4,5,6)	0 – 250 bar	± 1.25 bar
Crank angle decoder (Kistler 2614C / 720)	Determine CA	-360°÷+360°	± 0.23° CA

The in cylinder pressure sensors used in de compression ignition tests are of the type Kistler 7061B and connected to a data collecting unit of type Kistler Kibox Type 2893.Table 17 lists the specifications of these pressure sensors. The Kibox 2893 correlates crank angle to in cylinder-pressures via the decoder described in Table 18. The same in cylinder pressure sensors are used in the spark ignition test in cylinders 3,4,5 and 6.

Table 17: pressure sensor specifications used in the CI tests.

Parameter	Unit	Value
Range	[bar]	0-250 (± 1,25 bar)
Calibrated partial ranges	[bar]	
	[bar]	0-50
	[bar]	0-5
Overload	[bar]	300
Sensitivity	[pCbar^{-1}]	≈−80
Natural frequency	[kHz]	≈ 45
Linearity, all ranges	[% FSO]	≤±0.5
Acceleration sensitivity	[barg^{-1}]	<0.01
Operating temperature range	[∘C]	-50-350
Sensitivity shift		
cooled 50 ±35 [∘C]	[%]	≤±0.5
non-cooled 200 ±150 [∘C]	[%]	≤±2
Load-change drift	[bars^{-1}]	≤±0.5
Thermo shock		
at 1500 [min^{-1}], 9 [bar] IMEP		
Δp	[bar]	≤±0.1
Δ IMEP	[%]	≤±0.5
Δ $p$max	[%]	≤±0.5
Insulation resistance	[TΩ]	≥10
at 20 [∘C]		
Tightening torque	[Nm]	25
Cooling water pressure	[bar]	≤6
Capacitance (incl. cable)	[pF]	11 (117)
Weight	[g]	27
Plug, ceramic insulator		10-32 UNF

Table 18: crank angle decoder

Parameter	Unit	Value
Resolution of measurement data	[kHz]	312.5
	°CA	0.1
accuracy	°CA	±0,23 °CA
Speed range	[min^{-1}]	≈ 0 – 15624

A.1.3 Dewetron Dewe-2600

The Dewetron Dewe-2600 is used in the Spark ignited setup to collect and store all sensor data all sensor data excluding the Kibox data (Table 19).

Table 19: sensors connected to the DEWE-2600

Dewetron sensors	use	range	accuracy
In cylinder pressure sensor CAT	In cylinder pressure cylinder 1 and 2	0-150 bar	±3,25 bar
TC Model TE1260	air and exhaust gas temperatures	-40 °C ÷1000 °C	± 1.5 °C ±0.004*(T)
PT100	lubrication oil and cooling water temper-atures	-220 °C ÷ 600 °C	± 0.3 °C ± 0.005*(T)
Pressure sensor 10 bar	air pressures	0 ÷ 10 bar	± 0.02 bar
Flow sensor KRAL BEM 500	methanol flow	0 ÷ 300 kg/s	± 0.3 kg/s (±0.1%)

A.1.4 Coriolis meter

The Micro Motion ELITE CMF010M Coriolis Meter, 1/10 Inch (DN2), 316L Stainless Steel was used in the compression ignition setup. Table 20 gives the specifications of the Coriolis meter.

Table 20: Specifications of the flow meter

Parameter	Accuracy
Mass flow accuracy (Liquid)	±0.10[%] of rate
Mass flow repeatability (Liquid)	±0.05[%] of rate
Volume flow accuracy (Liquid)	±0.10[%] of rate
Volume flow repeatability (Liquid)	±0.05[%] of rate
Mass flow accuracy (Gas)	±0.35[%] of rate
Mass flow repeatability (Gas)	±0.20[%] of rate
Density accuracy (Liquid)	±0.0005 g/cm3 (±0.5 kg/m3)
Density repeatability (Liquid)	±0.0002 g/cm3 (±0.2 kg/m3)
Temperature accuracy	±1 °C (±0.5[%] of reading)
Sensor maximum working pressure	1,812 psig (125 bar)